Bioactive Materials 23 (2023) 53–68

Contents lists available at ScienceDirect

Bioactive Materials

journal homepage: www.keaipublishing.com/en/journals/bioactive-materials

Promoting oral mucosal wound healing using a DCS-RuB_2A_2 hydrogel based on a photoreactive antibacterial and sustained release of BMSCs

Wenxin Qi [a,b], Naijun Dong [a,b], Lingling Wu [a], Xueqi Zhang [a], He Li [c], Hao Wu [a], Natalie Ward [d], Jian Yu [e,f], He Liu [e], Jiao Wang [a,*], Xiaoyong Deng [g,**], Robert Chunhua Zhao [a,h,i,j,***]

[a] School of Life Sciences, Shanghai University, Shanghai, China
[b] School of Medicine, Shanghai University, Shanghai, China
[c] Beijing University of Chemical Technology, Beijing, China
[d] Banner Ocotillo Medical Center, 1405 S Alma School Rd, Chandler, AZ, 85286, USA
[e] Division of Endodontics, Department of Oral Biological and Medical Sciences, Faculty of Dentistry, University of British Columbia, Vancouver, V6T 1Z3, Canada
[f] The State Key Laboratory Breeding Base of Basic Science of Stomatology (Hubei-MOST) & Key Laboratory for Oral Biomedicine Ministry of Education, School and Hospital of Stomatology, Wuhan University, Wuhan, 430079, China
[g] School of Environmental and Chemical Engineering, Shanghai University, Shanghai, PR China
[h] Institute of Basic Medical Sciences Chinese Academy of Medical Sciences, School of Basic Medicine Peking Union Medical College, Beijing, China
[i] Centre of Excellence in Tissue Engineering, Chinese Academy of Medical Sciences, Beijing, China
[j] Beijing Key Laboratory of New Drug Development and Clinical Trial of Stem Cell Therapy (BZ0381), Beijing, China

ARTICLE INFO

Keywords:
Oral mucosa
Light-responsive
Hydrogel
DCS
BMSCs

ABSTRACT

The high occurrence rate and difficulties in symptom control are listed as the major problems of oral mucosal disease by medical professionals. Following the development of oral mucosal lesions, the oral microenvironment changes, immunity declines, and continuous bacterial stimulation causes wound infection. Traditional antibacterial drugs are ineffective for oral mucosal lesions. To overcome this problem, a light-responsive antibacterial hydrogel containing sustained-release BMSCs was inspired by the trauma environment in the oral cavity, which is different from that on the body surface since it mostly remains under dark conditions. In the absence of light, the hydrogel seals the wound to form a barrier, exerts a natural bacteriostatic effect, and prevents invasion by foreign bacteria. Simultaneously, mesenchymal stem cells are presented, and the released growth factors and other substances have excellent anti-inflammatory and angiogenic effects, which result in rapid repair of the damaged site. Under light conditions, after photo-induced shedding of the hydrogel, RuB_2A exerts an antibacterial effect accompanied by degradation of the hydrogel. Results in a rat oral mucosal repair model demonstrate that DCS-RuB_2A_2-BMSCs could rapidly repair the oral mucosa within 4 days. Sequencing data provide ideas for further analysis of the intrinsic molecular mechanisms and signaling pathways. Taken together, our results suggest that this light-responsive antibacterial hydrogel loaded with BMSCs can be used for rapid wound repair and may advance the development of therapeutic strategies for the treatment of clinical oral mucosal defects.

1. Introduction

Oral diseases are some of the most common occurring worldwide [1]. Among them, oral mucosal defects are a series of diseases caused by the shedding of inflammatory necrotic tissue [2], thereby affecting the oral mucosa and soft tissues including ulcerative lesions of oral mucosa represented by recurrent aphthous ulcers [3], which seriously affect the quality of patients' life. The causes of mouth ulcers are various and

Peer review under responsibility of KeAi Communications Co., Ltd.
* Corresponding author.
** Corresponding author.
*** Corresponding author. School of Life Sciences, Shanghai University, Shanghai, China.zhaochunhua@vip163.com
E-mail addresses: qiwenxin@shu.edu.cn (W. Qi), dongnaijun@shu.edu.cn (N. Dong), 19990510wll@shu.edu.cn (L. Wu), xueqizhang@shu.edu.cn (X. Zhang), 342552448@qq.com (H. Li), haow@shu.edu.cn (H. Wu), natt.a.ward@gmail.com (N. Ward), yujiandoctor@whu.edu.cn (J. Yu), endoliuhe@gmail.com (H. Liu), jo717@shu.edu.cn (J. Wang), xydeng@shu.edu.cn (X. Deng).

https://doi.org/10.1016/j.bioactmat.2022.10.027
Received 31 August 2022; Received in revised form 18 October 2022; Accepted 25 October 2022

complex, such as an imbalance in the oral microbiota [3], fatigue, stress, and complications from diabetes [4], and there exist many types of oral ulcers, which leads to difficulty in accurate diagnosis. Nevertheless, due to the dynamic environment of the oral cavity, there are few effective treatments [5].

The human oral cavity contains complex microbiota, changes in which are affected by many factors such as exogenous food intake, physical diseases, and drug treatment. An imbalance of microbiota in the oral cavity can trigger various oral mucosal diseases. *Candida albicans* can induce dysbiosis of mucosal bacteria, destroy oral immune defense, and cause oral infectious diseases [6]. Oral mucosal patch disease, represented by oral lichen planus, is caused by a disturbance in the level of fungi in the oral cavity [7,8]. Recurrent aphthous ulcers may be associated with an increase in *Escherichia coli* and a decrease in the abundance of *Streptococcus* [9], and infection of cytotoxic T lymphocytes by microbiota causes mucosal epithelial cell damage, leading to ulceration [10]. Studies have shown that probiotics promote oral epithelial wound healing and reduce proinflammatory cytokine secretion *in vitro*, which is beneficial for the treatment of oral lichen planus [11]. One study [12] found that most infections in the oral cavity are caused by endogenous oral bacteria that have overcome the host immune system or underlying defects in the innate or specific immune systems. *S. aureus* is a gram-positive member of the Firmicutes phylum, which is commonly found on cutaneous and mucosal surfaces in healthy mammalian hosts as a commensal organism. However, viral infection or immunodeficiency can lead to invasion and infection [13]. Another study showed that IL-17 signaling is required for initial barrier defense to *S. aureus* in oral mucosal infections. A further study reported the occurrence of a case of Lemierre syndrome secondary to an odontogenic infection in the context of necrotizing mediastinitis and anterior opticobacteria [14]; therefore, dynamic changes in oral microbiota may be an even more important initiator of oral disease.

Common products currently on the market for the treatment of oral ulcers are composed of hyaluronic acid as a hydrogel or mouthwash combined with other substances possessing healing and soothing properties [15]. Traditional formulations have several limitations: they are easily removed by tongue movement, remain in the mouth for only a short period of time [16], do not display simultaneous antibacterial and damage repair properties; and can not firm antibacterial properties and low cytotoxicity; therefore, the development of oral wound healing materials that promote tissue repair and possess broad-spectrum antibacterial effects is imperative. Owing to its broad-spectrum antibacterial effect and potential to promote wound healing, photodynamic therapy (PDT) has a favorable effect on local, superficial infections and is suitable for the treatment of oral ulcers [17]. Recent studies have shown that PDT treatment mediated by the photosensitizer, indocyanine green, can accelerate the healing of traumatic oral ulcers in rats [18].

Wound healing undergoes a continuous process of hemostasis, inflammation, proliferation, and structural remodeling of damaged tissue [19], involving multiple cell types and various biological processes; therefore, dressings that can quickly stop bleeding and possess antibacterial and anti-inflammatory properties are important for wound healing and the generation of granulation tissue. A variety of hemostatic materials have been developed, such as polyethylene glycol [20], chitosan [21,22], and nanoclay [23]. In addition, the inflammatory response often accompanies the process of hemostasis [24], and antioxidant and antibacterial effects, immune regulation, and angiogenesis all play anti-inflammatory roles [25]. Interestingly, hydrogel has been shown in multiple studies to display good biocompatibility for hemostasis, in addition to successful antibacterial and drug delivery [26–29]. Moreover, inflammatory responses affect the structural regeneration of tissue and are regulated by various cytokines and growth factors [30]. During wound healing, reducing the increase in pro-inflammatory cytokines (IL-6) and promoting the proliferation of endothelial cells (CD31) reduces pathological pain and accelerates repair.

Bone marrow-derived mesenchymal stem cells (BMSCs) have been shown to migrate to sites of injury and accelerate repair *in vivo* [31–34]. These cells are involved in all three phases of the wound-healing process, and can also enhance healing by immune modulation and production of growth factors, which enhance neovascularization and re-epithelialization, stimulate angiogenesis, and accelerate repair [35–37]. One case study reported that increased wound closure occurs following administration of MSCs due to accelerated dermal fibroblast and keratinocyte migration [38].

Chitosan (CS), a linear aminopolysaccharide composed of β (1–4) glycosidic linkages attached to glucosamine and N-acetylglucosamine units formed by the N-deacetylation of chitin [39], is a low-cost biological material. In recent years, CS has received extensive attention due to its excellent hemostatic efficacy, antibacterial effects, tissue adhesion, and biocompatibility [40–42]. The hemostatic mechanism of CS is mainly polycationic mucoadhesion; positively charged CS readily binds to negatively charged sialic acid on mucosa, red blood cells, and platelets, stimulating red blood cell adhesion, fibrinogen adsorption, platelet activation, and the coagulation cascade [43–45]. Moreover, CS has excellent antibacterial abilities due to the binding of its positively charged NH_3^+ groups to negatively charged bacterial surfaces [46–48]. N-alkylated CS was created by grafting alkyl groups onto the amino groups, which better promotes the activation and aggregation of platelets and red blood cells to further improve hemostatic efficiency [49,50]; however, the antibacterial activity of alkylated CS decreases as the substitution degree or carbon chain length increases [51]. In addition to the cationic antibacterial properties of CS, the grafted C-12 alkyl chains enhance the bacteriostatic properties by intercalating into the outer membrane of *E. coli* cells [52]. The surface, porosity, and hydrophobicity of N-alkylated CS nanofibrous membranes (NACS-NM) and the crosslinked structure of nanofibers can accelerate blood coagulation and platelet activation [53]. Moreover, recent studies have found that microneedle patches with a dodecyl CS (DCS) coating can anchor to the cell membrane and allow blood cells to coagulate, thereby rapidly promoting hemostasis [54]; therefore, this DCS hydrogel can be used as an excellent base material for intraoral wound repair.

Wound repair in the oral cavity is different from the skin surface. The oral cavity is always in a moist and dark environment with many microorganisms. Wound repair materials for oral mucosa must have certain adhesion and antibacterial properties [55]. Further, the toxicity of the material itself must be considered, in addition to whether it has good degradability and biocompatibility after entering the gastrointestinal tract. Functional polymers that can be photochemically manipulated by exogenous light have immense promise in materials science [56]. Photoresponsive units can be attached as pendant groups or incorporated into the main chain of photocleavable polymers, which degrade to smaller molecules during a light-driven response. Photocleavable polymers also have significant potential in biological applications, particularly in the spatiotemporal patterning of cellular microenvironments in tissue engineering, smart drug-delivery, and diagnostic systems [57,58]. The dark environment of the oral cavity also provides natural conditions for light-responsive materials. The inspiration for the present study also stems from this fact; a photoactive ruthenium crosslinker enabled the creation of a hydrogel that responds with unique speed and efficiency to visible light exposure. Silver nanoparticles (Ag NPs) have been shown to prevent the growth and reproduction of many bacteria, such as *Bacillus cereus*, *Staphylococcus aureus*, *Escherichia coli*, *Klebsiella pneumoniae*, and *Candida albicans*, through the binding of Ag to biomolecules present in bacterial walls [59–61]. In addition, it has been proposed that Ag NPs generate reactive oxygen species and free radicals, which lead to apoptosis and prevent their replication. Ruthenium, as a metal cation, may also play a role in killing microorganisms in a similar manner within the same concentration range as Ag. Various Ru-based DNA photocleavers are known to damage DNA through an oxidative mechanism [62]. Different positively charged Ru(II) polypyridyl complexes have been demonstrated to bind to the negatively charged outer membrane of gram-negative bacteria

and intercalate the dppn ligand into the membrane [63,64]. In the present study, CS and the photocrosslinking agent Ru bipyridine were used to synthesize photoresponsive hydrogels. The picolinaldehyde group is shed after visible light irradiation, and Ru bipyridine plays a bactericidal role in the humid environment. Moreover, Ru-crosslinked polymer systems provide even greater spatiotemporal control over material properties, such as storage modulus and porosity, as well as the regulation of drug delivery profiles and cellular function in biomedical applications. Therefore, this light-responsive hydrogel can be regarded as a good stem cell presentation system. Under dark conditions, the material has no killing effect and its 3D structure is conducive to the growth and sustained release of BMSCs. This light-responsive antibacterial hydrogel capable of presenting BMSCs has broad application prospects in the wound repair of oral mucosa.

2. Results and discussion

2.1. The preparation and application of the DCS-RuB_2A_2-BMSCs hydrogel

The base material of the hydrogel was chitosan, and dodecylaldehyde was used to replace the amino group, obtaining dodecyl chitosan (DCS). The molar ratio of the raw materials was set as 0.4:1 to achieve the best hemostatic performance of DCS and simultaneously aid platelet aggregation and red blood cell adsorption. $Ru(bpy)_2Cl_2$ solution was refluxed at 80 °C for 5 h under argon protection, after which Cl was replaced with 3-pyridinecarboxaldehyde. The material was separated, evaporated to dryness, and purified to obtain a brown-black solid, which was subsequently dissolved in water to yield Ru(bipyridine)$_2$(3-pyridinecarboxaldehyde)$_2$ (RuB_2A_2: B is 2,2′-bipyridine and A is 3-pyridinecarboxaldehyde). Under acidic conditions, DCS and RuB_2A_2 undergo a Schiff base crosslinking reaction to form a dense network-like gel. The amide bond formed by the crosslinking of DCS and RuB_2A_2 greatly enhances the performance of the gel. Under light irradiation, 3-pyridinecarboxaldehyde falls off, the DCS-RuB_2A_2 hydrogel decomposes, and DCS and RuB_2A/RuB_2 act independently. The dodecyl group of DCS anchors the bacterial outer membrane, and the released RuB_2A/RuB_2 attaches to the cell surface and causes changes in cell permeability, resulting in the escape of cellular components and interference with the role of enzymes in cellular metabolism. At the same time, RuB_2A/RuB_2 ruptures the membrane and causes damage to DNA, thereby exerting a bactericidal effect. Following application of DCS-RuB_2A_2-BMSCs to oral mucosal defects, the hydrogel firstly attaches to the wound and DCS causes rapid hemostasis and platelet aggregation. Under dark conditions, the hydrogel slowly releases BMSCs and the cytokines in the BMSCs microenvironment play an anti-inflammatory role, as well as promoting the formation of new blood vessels. After the slow release of BMSCs into the wound environment, the hydrogel can be irradiated with a light source to exert an antibacterial effect.

2.2. Characterization of DCS-RuB_2A_2

To achieve rapid hemostasis and a synergistic antibacterial light-responsive hydrogel system, we first performed dodecyl substitution of common CS. Previous research [49] has shown that alkyl substitution can enhance platelet activation and blood cell adsorption. Scanning electron microscopy (SEM) analysis was performed to characterize the microstructure of the hydrogel (Fig. 2A–D). CS was fragmented, with a flat, smooth surface and a small number of pores, whereas DCS had markedly more pores and the gel was flocculent. This sponge-like structure greatly enhances the adsorption effect.

The chemical structures of CS and DCS were characterized by Fourier transform infrared spectroscopy (FTIR) (Fig. 2E). In the original CS sample, the vibrational –OH group peak of the glycopolymer (approximately 3440 cm^{-1}) and the stretching peak of the methyl and methylene groups (approximately 2800–2900 cm^{-1}) can be observed. Furthermore, the three typical vibrational peaks of CS, the stretching vibration of the –CO bond (approximately 1640 cm^{-1}), the bending vibration of the $–NH_2$ group (approximately 1580 cm^{-1}), and the symmetric vibration of the –CN bond (approximately 1310 cm^{-1}) can also be seen. In comparison with CS, DCS displays a clear absorption peak at 2800–2900 cm^{-1}, with a more pronounced $–CH_2$ antisymmetric stretching peak (approximately 2920 cm^{-1}) and a significantly stronger $–CH_3$ antisymmetric stretching peak (approximately 2850 cm^{-1}). DCS shows no peak at 2810–2720 cm^{-1}, indicating that the alkyl aldehyde impurity has been removed. The amino absorption peak (approximately 1580 cm^{-1}) is weaker, while the –NH bond absorption peak (approximately 1560 cm^{-1}) is significantly enhanced. Moreover, the $–CH_2$ and $–CH_3$ variable angle bending vibration peaks (approximately 1460 cm^{-1}) are also present, suggesting linkage of the alkyl group to the amino group of CS and the synthesis of DCS (Fig. 2E). Previous literature [65] has demonstrated that different aldehyde group substitutions greatly affect the hemostatic properties of CS; therefore, we speculated that other substitutions may show better effects. By changing the molar ratio of dodecanal to CS, DCS with differing degrees of substitution was generated. Additionally, the strength of these bending, vibrational, and tensile peaks was also directly related to the different feeding ratios, and the intensity of the –NH bending vibration peak increased as the molar ratio of dodecanal to CS became higher. These data indicate that the alkyl group is successfully linked to the amino group on CS and that the intensity of the characteristic peak of groups varied with the molar ratio (Fig. 2F). Fig. 2G is a photograph of the hydrogels of DCS with differing degrees of substitution.

To generate an effective, visible light-responsive hydrogel system, we synthesized a photorelease crosslinker, Ru(bipyridine)$_2$(3-pyridinecarboxaldehyde)$_2$ (RuB_2A_2. B is 2,2′-bipyridine and A is-pyridinecarboxaldehyde, Fig. 1, Fig. 2H). NMR results demonstrated successful synthesis of RuB_2A_2 (Supplementary Fig. 1). RuB_2A_2 undergoes substitution of a single pyridine in water to yield $RuB_2A(H_2O)$ and free ligand A, a process which occurs in less than 120 s (Fig. 2I, J) and conforms to the Ru(II) polypyridyl complex shedding process described in the literature [58,66]. Fig. 2I demonstrates that RuB_2A_2 substitution occurs in a manner typical for a metal-to-ligand charge transfer (MLCT) and displays comparable spectra to those of known Ru (II) polypyridyl complexes. The UV–Vis absorption spectra suggest that photoreaction cleaves one ligand, resulting in red shift of the absorption peak from 446 nm to 469 nm RuB_2A_2 exhibits strong absorbance to 510 nm, with a tail extending past 560 nm. The peak wavelength map (Fig. 2J) can be divided into two stages: the first stage (0–120 s) is attributed to the photorelease of the first 3-pyridinecarboxaldehyde, and the second stage corresponds to the stable state of the single chain RuB_2A.

By analyzing changes in the peak wavelength of RuB_2A_2 with illumination time, the results show that the peak wavelength of RuB_2A_2 tends to be stable after 120 s of illumination, suggesting complete photolysis of only one Ru–pyridine bond (Fig. 2J). HPLC analysis following the photodegradation of the crosslinker further confirmed the photolysis products as $RuB_2A(H_2O)$ and free ligand A (Fig. 2K).

RuB_2A_2 has a good crosslinking reaction with DCS, which is attributed to the fact that the aldehyde group of ligand A in RuB_2A_2 can undergo a Schiff base reaction with the amino group of DCS under acidic or basic conditions to form better mechanical properties. In addition to the adhesive hydrogel (Fig. 2H), the hemostatic properties of DCS are retained and there is also a good photoresponse effect. SEM analysis was performed to characterize the microstructure of the DCS-RuB_2A_2 hydrogel (Fig. 2L and M). The structure of the crosslinked RuB_2A_2 hydrogel is obviously denser, indicating better mechanical properties, which are closely related to the plasticity and adhesion properties of the gel in Fig. 2H. The FTIR results of RuB_2A_2 and DCS crosslinked with Ru (bipyridine)$_2$(3-pyridinecarboxaldehyde)$_2$ (DCS-RuB_2A_2) are shown in Fig. 2N. EDX analysis demonstrates that the Ru element has been successfully crosslinked to the DCS hydrogel (Fig. 2O–Q).

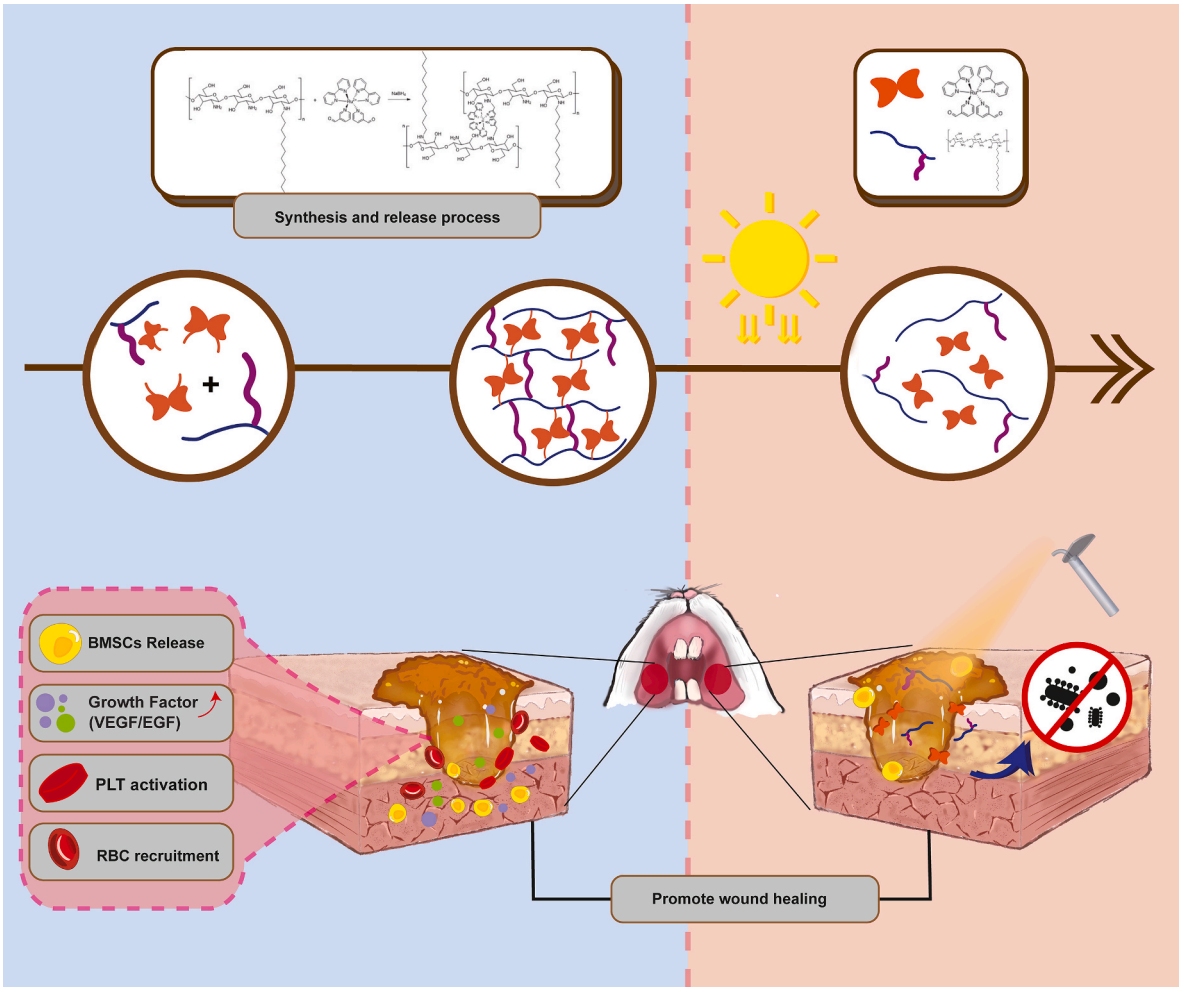

Fig. 1. Schematic showing the preparation and application of the DCS-RuB_2A_2-BMSCs hydrogel.

2.3. Coagulation and hemostatic properties of DCS

To determine the hemostatic properties of DCS-RuB_2A_2, a model of hemostasis in the mouse tail was employed (Fig. 3A). It can be seen that the bleeding volume in the materials group following treatment of the tail wound is significantly less than that in the gauze group, and the hemostatic effect of DCS is better than that of CS. The hemostasis time and amount of blood loss for each group are shown in Fig. 3C and D. These results demonstrated that as the substitution degree of aldehyde groups in DCS increases, the bleeding volume and hemostasis time decreases and subsequently gradually increases, and the hemostatic effect was best at a substitution degree of 0.4 DCS. Blood clotting time (BCT) was used to measure the blood coagulation properties of the materials. Blood flowed freely when extracted from the vessel; however, under the action of the hemostatic material, the blood clotted and formed a stable clot. Fig. 3B shows the state of blood coagulation after treatment with different materials. It can be seen that the blank group (blood only) is not completely coagulated despite being left to stand for a long time. An obvious stratification phenomenon is formed between CS, 0.1 DCS, and 0.2 DCS, which may be due to the small intermolecular space, which cannot deeply adsorb blood. Encouragingly, 0.3 DCS, 0.4 DCS, and 0.6 DCS are all infiltrated by blood, similar to the gel sponge, which can absorb all the blood in the pores of the gel molecules, thus exerting the effect of rapid coagulation. Fig. 3E shows that the time for the CS group to form a blood clot was approximately 400 s, while that for 0.4 DCS was no longer than 100 s. It can be clearly observed that 0.4 DCS had a much stronger promoting effect on clotting than CS, and the difference between 0.4 DCS and CS was significant ($p < 0.0001$).

2.4. In vitro antibacterial performance

To further explore the antibacterial ability of RuB_2A_2, the potential antimicrobial activities of RuB_2A_2 were investigated using *Escherichia coli* and *Staphylococcus aureus*. Following the addition of RuB_2A_2 to co-cultures of *E. coli* and *S. aureus*, SEM characterization of the bacterial surface was markedly altered, and objects appeared to be attached to the surface, in addition to some of the bacterial contents being extracellular (Fig. 4A). This suggests that RuB_2A_2 attaches to the cell membrane of bacteria, changing the permeability of the cell membrane and allowing part of their contents to escape, thereby exerting a bactericidal effect. Different concentrations of RuB_2A_2 and bacteria were mixed and spread on a nutrient agar plate (Fig. 4B). After culture at 37 °C for 18 h, the number of *E. coli* (Fig. 4C) and *S. aureus* (Fig. 4D) were counted. An obvious antibacterial effect can be observed at a concentration of 0.125 mg/mL RuB_2A_2. As the concentration of RuB_2A_2 increases, the antibacterial ability is gradually enhanced, but the inhibitory effect on *E. coli* is higher than that on *S. aureus*. In conjunction with the results of the subsequent cytotoxicity test, it can be seen that at a concentration of 0.125 mg/mL, RuB_2A_2 significantly inhibits the growth of two representative bacteria but has little effect on cell viability; therefore, this concentration of RuB_2A_2 was used in the hydrogel for successful biocompatibility and antibacterial properties. Subsequently, the effect of different treatments on the antibacterial properties of the hydrogels was explored using the zone of inhibition (ZOI) method (Fig. 4E). The

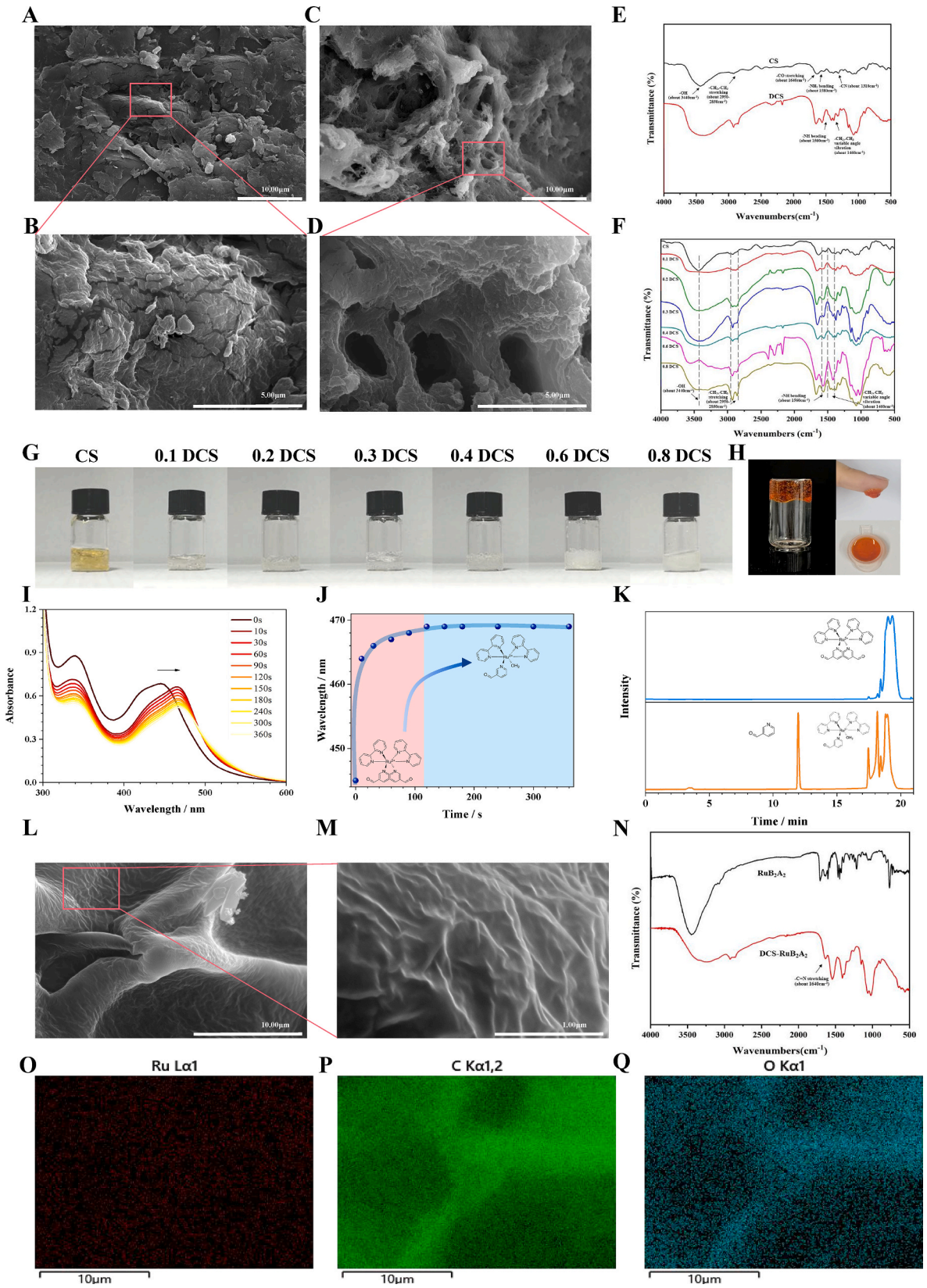

Fig. 2. Performance characterization of DCS-Ru_2BA_2 and exploration of the crosslinking mechanism. SEM images of CS (A, B) and DCS (C, D); scale bars 10 μm and 5 μm. (E) FTIR spectra of CS and DCS. (F) FTIR spectra of DCS with differing degrees of substitution. (G) Photographs of CS and DCS. (H) Photographs of DCS-RuB_2A_2. (I) UV–Vis spectral evolution of RuB_2A_2 (100 μmol L^{-1}) in deionized water with increasing irradiation time (λex = 450 nm, 14 mW cm^{-2}). (J) The wavelength corresponding to the UV absorption peak of RuB_2A_2 varies with illumination time. Pink represents the first stage and blue represents the second stage. (K) HPLC analysis of the photodegradation of crosslinkers under dark conditions (blue) and after illumination (orange). (L, M) SEM images of DCS-RuB_2A_2; scale bars 10 μm and 1 μm. (N) FTIR spectra of DCS-RuB_2A_2. (O-Q) Mapping images of C, O, and Ru elements of DCS-RuB_2A_2 in (L).

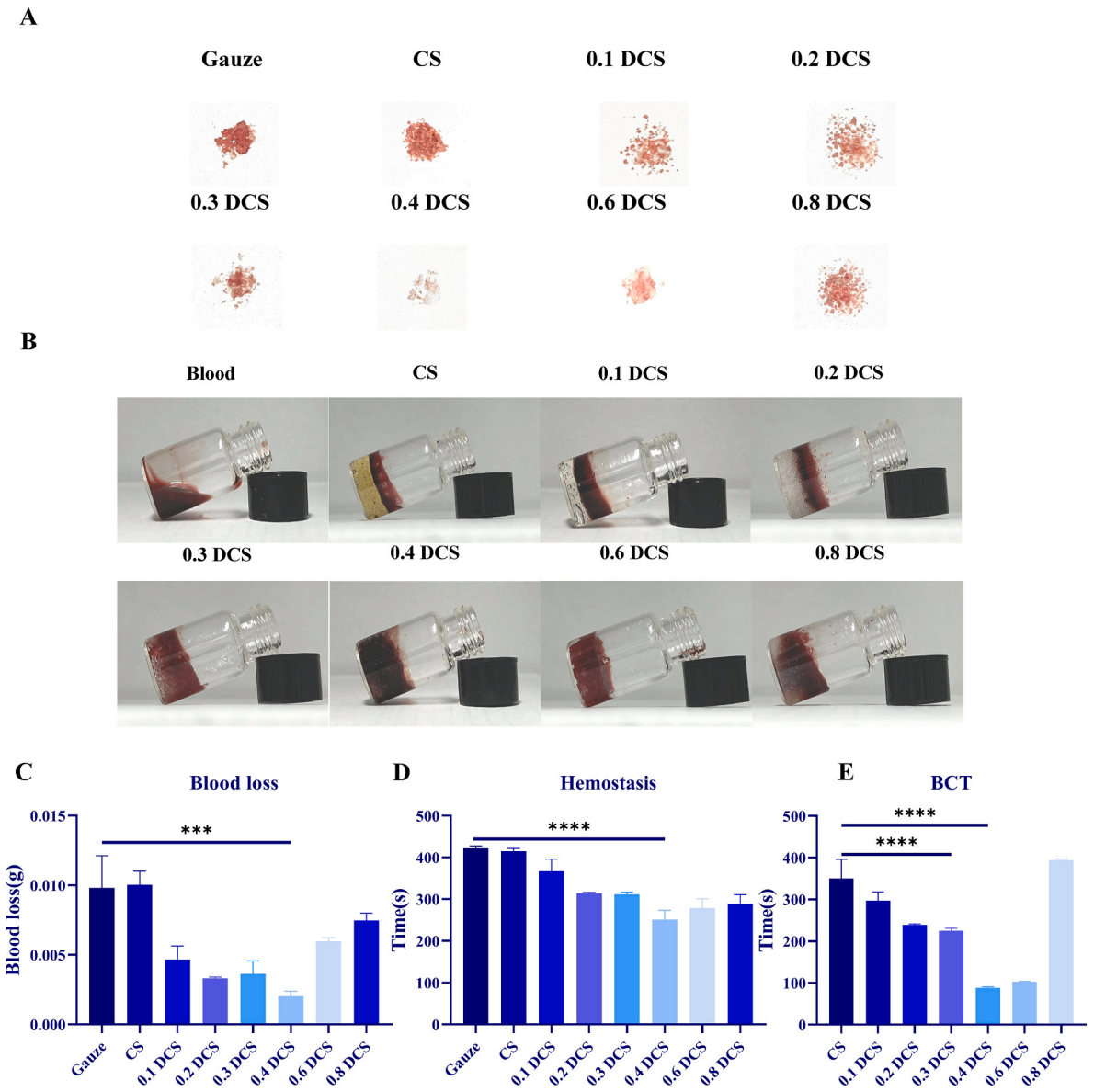

Fig. 3. Coagulation and hemostatic properties of DCS. (A) Photographs of blood loss after tail docking in mice. (B) *In vitro* coagulation profiles following treatment with CS and DCS with differing degrees of substitution. (C) Histogram of blood loss in mice. (D) Histogram of hemostatic time in mice. (E) Statistical histogram of blood clotting time. ($n \geq 3$, $^{*}p < 0.05$, $^{**}p < 0.01$, $^{***}p < 0.001$, $^{****}p < 0.0001$).

inhibitory effect of RuB_2A_2-DCS on *E. coli* (Fig. 4F) and *S. aureus* (Fig. 4G) under light conditions was significantly greater than that of the other groups, and the inhibitory effect on *S. aureus* was stronger. This indicates that light is necessary for RuB_2A_2-DCS to exert a bacteriostatic effect.

2.5. Cytocompatibility of DCS-RuB_2A_2

The biosafety of DCS-RuB_2A_2 is crucial for the use of hydrogels as wound hemostasis and healing dressings. HEK 293T, adherent-dependent epithelioid cells, were used here as a model to mimic oral epithelial cells *in vitro*. Cytotoxicity was assessed by exposing HEK 293T cells to CS (control group) and differing substitution degrees of DCS in leaching solution for 24 h and 48 h. After treatment, cell viability was measured using a Cell Counting Kit-8 (CCK-8). Fig. 5A and B shows that both CS and DCS have good biocompatibility. In particular, after 48 h of coculture, the viability of cells treated with CS did not change significantly as compared with that at 24 h; however, the viability of cells treated with 0.4 DCS (degree of substitution) was improved to approximately 100%. RuB_2A_2 was crosslinked to our light-responsive material and shown to have a good bacteriostatic effect (Fig. 4 B–G). It was necessary to further explore the optimal concentration at the level of epithelial cells. HEK 293T cells were cultured in the presence of different concentrations of RuB_2A for 24 h and 48 h under light conditions. RuB_2A at a concentration of no more than 0.5 mg/mL shows good biocompatibility after 24 h, with a cell viability of higher than 50%. After 48 h, the cytotoxicity in the group treated with RuB_2A at a concentration of less than 0.125 mg/mL is still within an acceptable range (Fig. 5C and D). For a more insightful observation of cell survival, Hoechst 33342 and Propidium Iodide (PI) staining was used to differentiate between live and dead cells. Hoechst 33342 can penetrate cell membranes to label live cells with green fluorescence, but PI cannot penetrate or stain normal cells with intact cell membranes. In the case of necrotic cells, the integrity of their cell membranes is lost and they can be stained red. The survival rate and number of dead cells were detected 24 h after treatment with different concentrations of RuB_2A. Fig. 5G and Supplementary Fig. 2 shows that at concentrations below 0.125 mg/mL, RuB_2A has a negligible effect on cell viability. Comprehensively

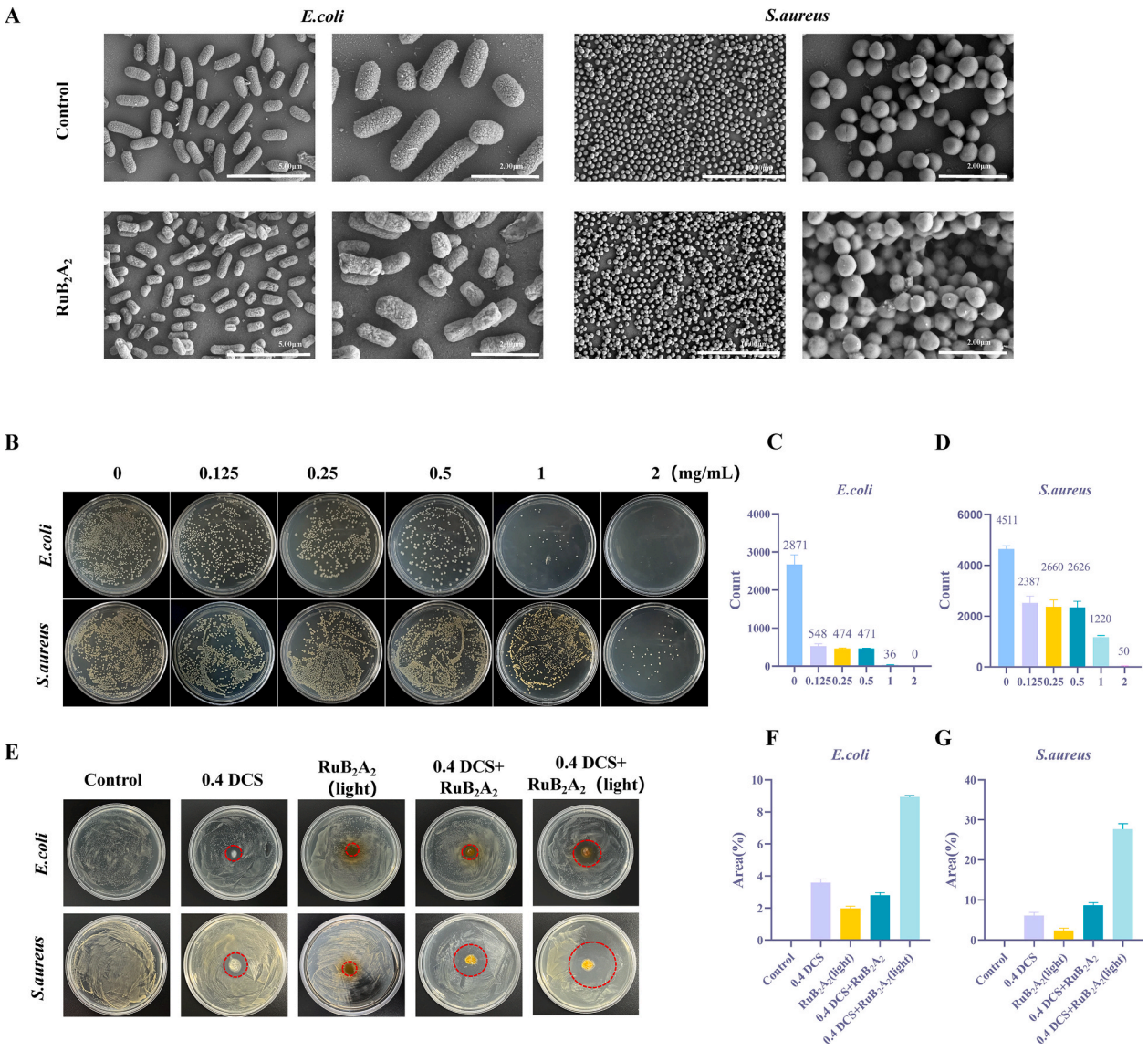

Fig. 4. *In vitro* antibacterial performance. (A) SEM images of *E. coli* and *S. aureus* treated with the control and RuB_2A_2. (B) Growth of *E. coli* and *S. aureus* with different concentrations of RuB_2A_2 added to the agar plates. Colony numbers of *E. coli* (C) and *S. aureus* (D). (E) ZOI method to test the effect of light on the antibacterial properties of the hydrogel and its components. The areas of the inhibition zone for *E. coli* (F) and *S. aureus* (G) in each group were counted.

considering the bacteriostatic effect and cytotoxicity, 0.125 mg/mL is considered the optimal concentration that produces minimal toxicity to normal cells in the long-term and also displays a certain bacteriostatic effect. Since the oral environment is mostly under dark conditions, the antibacterial effect of DCS-RuB_2A_2 under non-light conditions was general (Fig. 5E and F). RuB_2A formed by picolinaldehyde shedding after illumination exerts an antibacterial effect. HEK 293T cells were cultured in the presence of 0.4 DCS for 24 h and 48 h to explore the effect of light on cell viability. In comparison with the control and DCS-treated groups, the cell viability of the DCS-RuB_2A_2-treated and DCS-RuB_2A (light)-treated groups is decreased. The cell viability following DCS-RuB_2A_2 treatment is 80–90% at both 24 h and 48 h under dark conditions, while that following DCS-RuB_2A (light) treatment is slightly lower at 75–85%. It can be seen that the light conditions significantly reduce cell viability, indicating that DCS-RuB_2A_2 has a good light-controlled effect and the oral environment will not affect the normal epithelium. Material have lower cytotoxicity and good biocompatibility, which is the premise of hydrogels as wound healing dressings in the oral cavity.

2.6. Paracrine effects of BMSCs

In recent years, stem cells have been shown to benefit angiogenesis through paracrine action, and at the same time, they can release cytokines, growth factors, chemokines, and extracellular vesicles to promote tissue regeneration and repair. Accordingly, to accelerate the healing of oral mucosal defects, BMSCs were loaded onto DCS-RuB_2A_2, and the loose and hollow properties of the hydrogel provided a 3D structure more conducive to their growth and release of cytokines. BMSCs were co-cultured with HEK 293T cells (Fig. 6A) to explore the effect of the BMSCs microenvironment on the growth, proliferation, and migration of epithelial cells. The CCK8 assay was used to evaluate the proliferative ability of HEK 293T cells by detecting the OD values at 6 h, 12 h, 24 h, 36 h, and 48 h. The results show that the proliferation ability of HEK 293T cells co-cultured with BMSCs is significantly increased, suggesting that the microenvironment of BMSCs is conducive to the growth and proliferation of epithelial cells (Fig. 6B). The cell scratch assay was used to test cell migration ability in the presence of BMSCs, and Fig. 6C and D demonstrates that the size of the wound healing area between cell scratches was significantly lower than that of the control group,

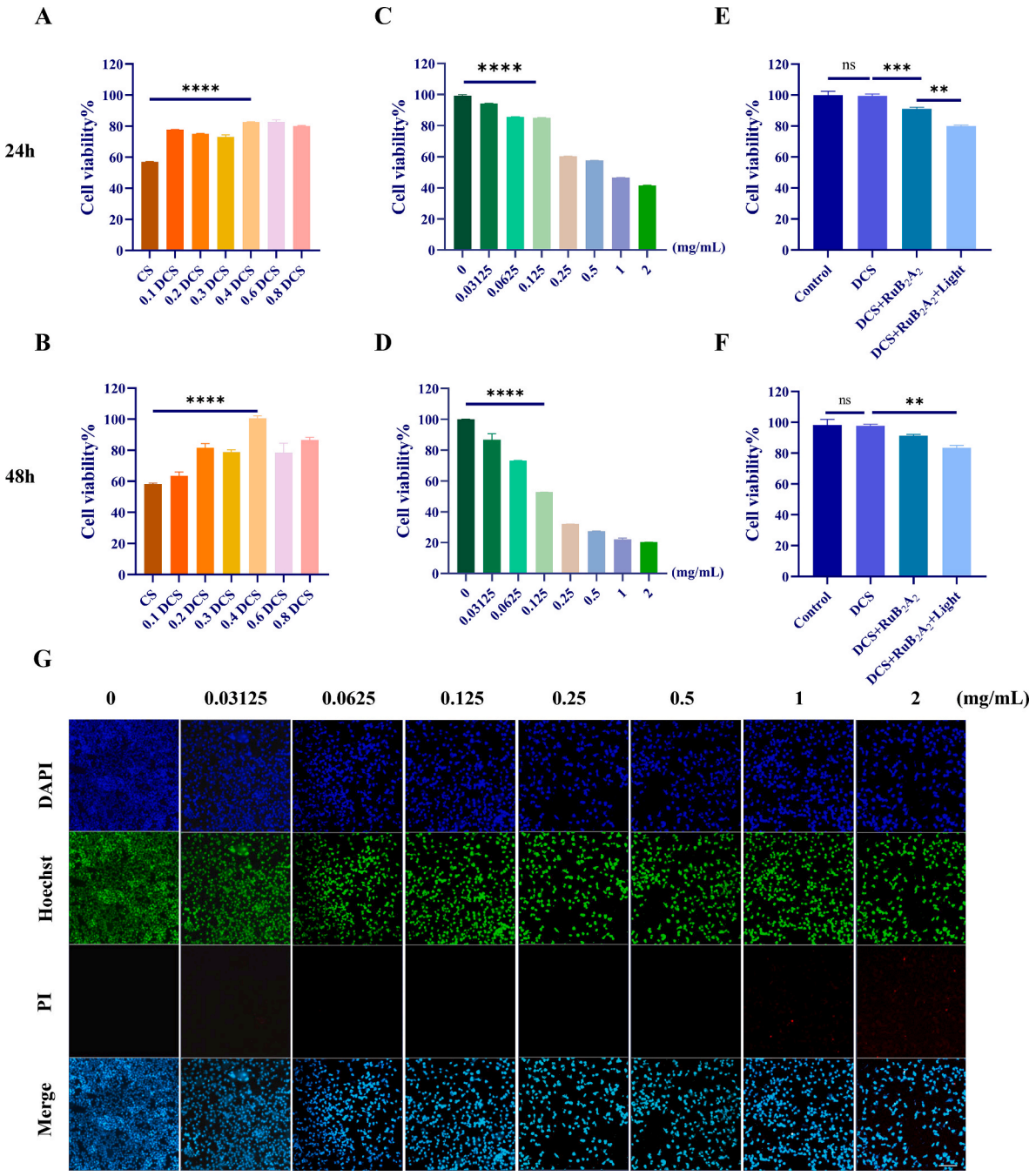

Fig. 5. Cytocompatibility of DCS-RuB$_2$A$_2$. The CCK-8 method detected the cytotoxicity of CS and DCS with differing degrees of substitution (A, B) and RuB$_2$A$_2$ at different concentrations (C, D). (E, F) CCK-8 assays for the biocompatibility of DCS-RuB$_2$A$_2$ under light and dark conditions. (G) (PI/Hoechst) live and dead cell staining images and statistical analysis of HEK 293T cells cultured for 24 h, scale bars 50 μm (n ≥ 3, *$p < 0.05$, **$p < 0.01$, ***$p < 0.001$, ****$p < 0.0001$).

suggesting that the microenvironment of BMSCs significantly enhances the migration ability of epithelial cells. Lipopolysaccharide (LPS) is an inflammatory stimulator often used to construct cellular inflammatory models. To explore the BMSCs paracrine effect on epithelial cells, an inflammatory model of HEK 293T cells was constructed using an appropriate concentration of LPS, following which BMSCs were cocultured. The expression levels of transforming growth factor beta (TGF-β), platelet-derived growth factor (PDGF), epidermal growth factor (EGF), fibroblast growth factor (FGF), and vascular endothelial growth factor (VEGF) were measured. Interestingly, the mRNA expression levels of TGF-β, PDGF, EGF, FGF, and VEGF were significantly increased following stimulation by the BMSCs microenvironment (Fig. 6E–I), demonstrating that BMSCs can rapidly elevate the expression of growth factors in a short period of time to promote the regulation of downstream signaling pathways, a mechanism that provides the possibility for the rapid healing of oral wounds.

2.7. Application of DCS-RuB$_2$A$_2$-BMSCs to promote mucosal defect healing in a rat model

To determine the *in vivo* wound closure efficacy of the photoresponse hydrogels containing BMSCs, oral mucosal defects were created in the mouths of rats and an infection was established with *E. coli* and *S. aureus*. Subsequently, 1×10^4 BMSCs were resuspended in 10 μL PBS, injected into 3g DCS-RuB$_2$A$_2$ hydrogel, and allowed to incubate in the dark for 2 min. The prepared samples were applied at the wound sites (Fig. 7A).

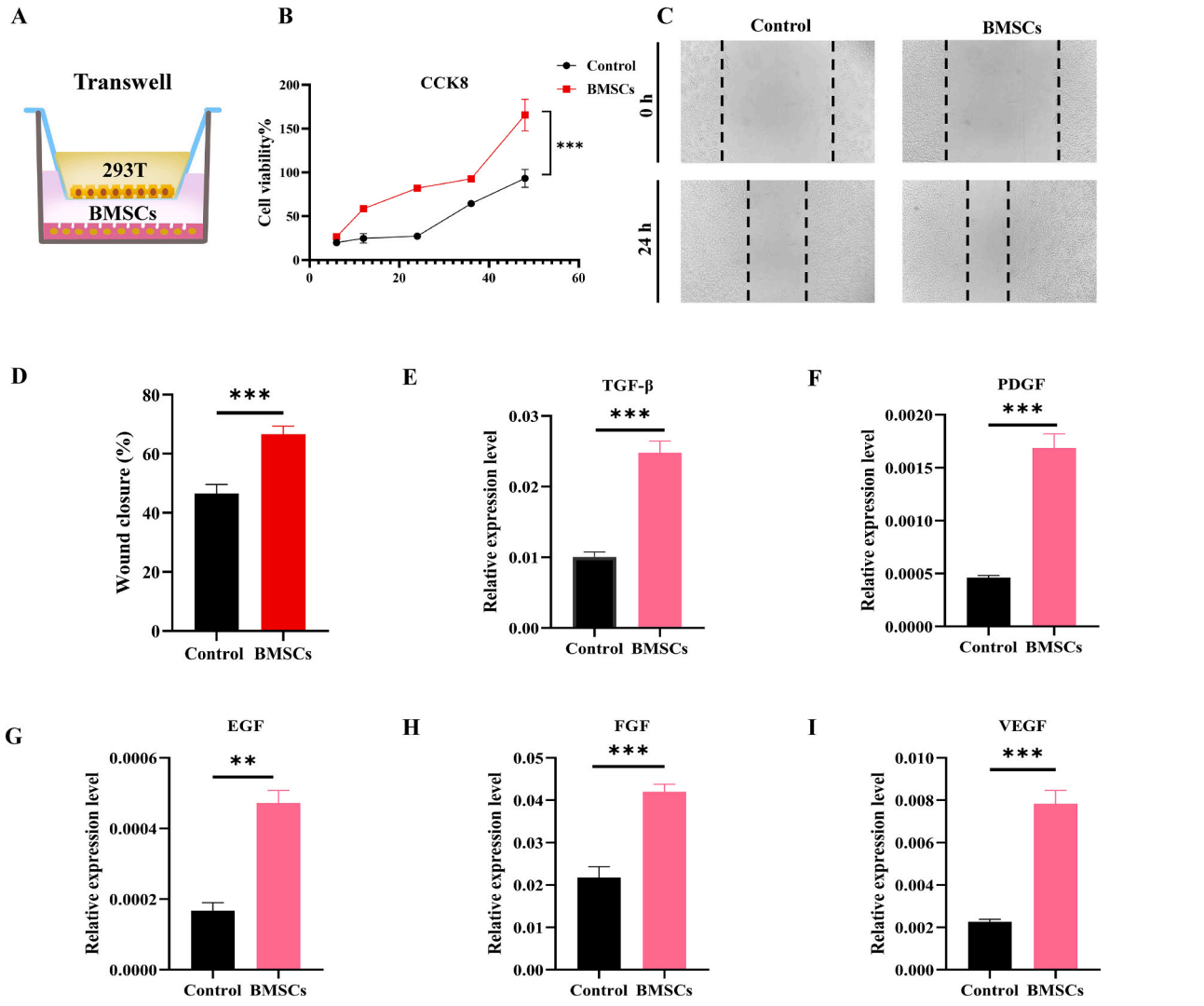

Fig. 6. Paracrine effects of BMSCs. (A) Schematic diagram of the co-culture of BMSCs and HEK 293T cells. (B) CCK-8 assay to detect cell viability after co-culture of HEK 293T cells and BMSCs. (C) Cell scratch assay to detect the cell migration ability of HEK 293T cells after co-culture with BMSCs. (D) Statistical histogram of the cell migration ability after BMSCs co-culture. (E–I) Growth factor expression levels in HEK 293T cells after co-culture with BMSCs ($n \geq 3$, $^{*}p < 0.05$, $^{**}p < 0.01$, $^{***}p < 0.001$, $^{****}p < 0.0001$).

Fig. 7B shows images of the oral mucosal defects taken at different time intervals after treatment with the control and DCS-RuB_2A_2 hydrogels in the presence and absence of BMSCs. There is no sign of inflammation or infection in the DCS-RuB_2A_2-BMSCs-treated group and growth of new oral mucosa can be observed, which resulted in a reduced wound area. On day 4, the wounds treated with DCS-RuB_2A_2-BMSCs and DCS-RuB_2A_2 were almost completely healed and the oral mucosa was closed, whereas the control group still had obvious oral mucosal defects. In particular, the oral mucosa in the DCS-RuB_2A_2-BMSC-treated group became very smooth after healing. Interestingly, DCS-RuB_2A_2-BMSCs and DCS-RuB_2A_2 both had valuable wound closure effects in comparison with the DCS and control groups; therefore, both DCS-RuB_2A_2 and BMSCs can enhance wound healing *in vivo*. The results in Fig. 7C show that on day 4, the wounds treated with DCS-RuB_2A_2-BMSCs were significantly reduced as compared with the control. These results may be due to the material properties of DCS-RuB_2A_2 hydrogels, such as the antibacterial and platelet recruitment effects, which can enhance adhesion at the wound site, promoting wound contraction and closure during the early stages of the wound healing process. Moreover, the introduction of BMSCs promoted the release of many cytokines, which rapidly accumulate at the site of inflammation and promote repair, which is beneficial for reduced infection in the wound area during the initial stages of healing.

Furthermore, following treatment with different materials, the mucus was extracted from the oral wound into the medium and cultured for 8 h at 37 °C. Although external adverse stimulation is one of the main causes of inflammation, fewer bacteria were detected in the DCS-RuB_2A_2-BMSCs- and DCS-RuB_2A_2-treated groups (Fig. 7D and E).

To further investigate the biological mechanism of the wound healing process, hematoxylin-eosin (H&E) staining and immunohistochemical analysis were performed on mouse wound tissue sections. Wounds on day 4 of being covered with DCS-RuB_2A_2-BMSCs and the other samples are shown in Fig. 8A. The surface of wounds treated with DCS-RuB_2A_2-BMSCs and DCS-RuB_2A_2 show complete formation of new epithelium, while the control group still shows obvious oral mucosal defects as observed by H&E staining (Fig. 8A). As the main component of the extracellular matrix, collagen binds to cell surface receptors and participates in signal transduction processes. In addition, collagen plays an important role in cell proliferation, migration, differentiation, and other cellular activities to promote adhesion, movement, growth, and deposition of cells on new connective tissue. At the same time, collagen induces chemotaxis of fibroblasts to accelerate wound repair and improve the quality of wound healing [67]. After 4 days of treatment, retrieved tissues were subjected to Masson's trichrome staining to identify collagen (Fig. 8A). It can be seen from the intensity and area of

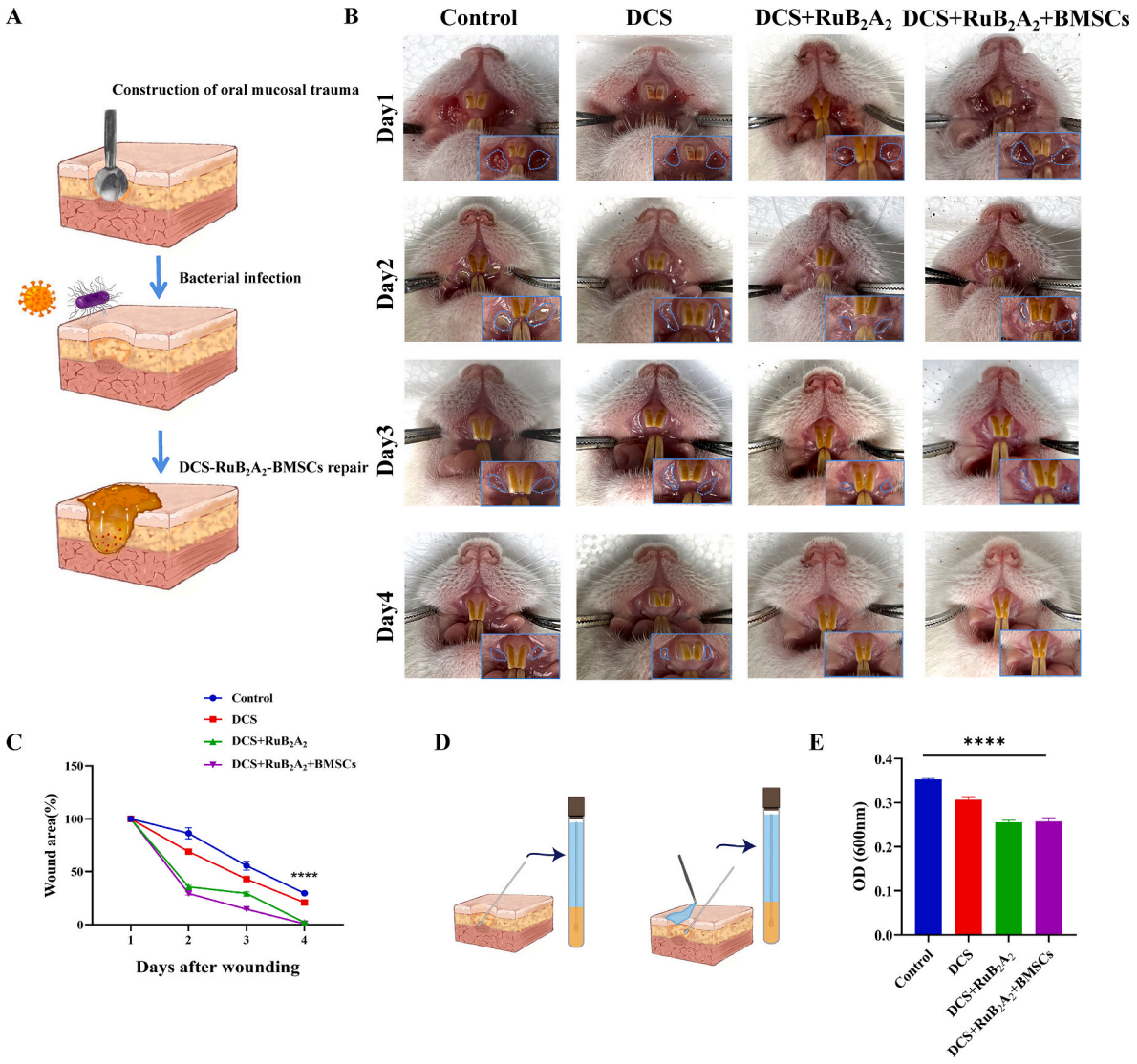

Fig. 7. Application of DCS-RuB$_2$A$_2$-BMSCs to promote mucosal defect healing in a rat model. (A) Schematic diagram of the construction of the rat oral mucosal defect model. (B) Photographs of oral mucosal defects in rats. (C) The wound area in (B) was measured. (D) Schematic diagram of the local bacterial culture of the extracted affected area. (E) OD values for the bacterial cultures at 600 nm after 8 h ($n \geq 3$, $^{*}p < 0.05$, $^{**}p < 0.01$, $^{***}p < 0.001$, $^{****}p < 0.0001$).

blue staining that there are significant differences in collagen deposition among the experimental groups. The DCS-RuB$_2$A$_2$-BMSCs group has the highest collagen deposition, indicating that this material has the best wound healing effect. Furthermore, DCS-RuB$_2$A$_2$-BMSCs-treated wounds display more densely packed collagen fibers in the extracellular matrix, which is in contrast to other samples that display loosely packed collagen fibers.

Cytokines such as IL-6, TNF-α, and platelet endothelial cell adhesion molecule-1 (CD31) play an important role in the process of wound healing. Immunohistochemistry was used to explore the regulation of cytokines by incorporated BMSCs. As shown in Fig. 8B and C, in comparison with the control group, the levels of IL-6 and TNF-α are significantly reduced in the DCS-RuB$_2$A$_2$-BMSCs group. At this time, the wound has entered the mature stage of healing and the inflammatory factors are reduced. On the contrary, the control group is still in the inflammatory or proliferative stage, in which the levels of IL-6 and TNF-α remain high. Treatment with DCS-RuB$_2$A$_2$-BMSCs greatly accelerates wound healing. The process of wound repair is accompanied by the formation of granulation tissue and deposition of collagen, and the formation of new blood vessels is also indispensable. CD31 is an angiogenesis marker, staining and quantitative analysis of which (Fig. 8A and D) show that DCS-RuB$_2$A$_2$-BMSCs promotes the production of CD31 in wound tissue, and the blood vessel density is significantly increased as compared with that in the other groups. These results indicate that the risk of infection is reduced during the early stages of wound healing due to hemostasis initiated by DCS, in addition to the recruitment of platelets and the antibacterial effect of RuB$_2$A$_2$. The incorporation of BMSCs improves the production of cytokines and chemokines around the wound and simultaneously stimulates angiogenesis, providing a low-inflammatory environment to enable wound repair to rapidly enter the proliferative stage of healing. Moreover, fibroblasts are derived from mesenchymal stem cells, which can produce a large amount of collagen, promoting the repair of wounds and aiding rapid recovery in approximately 4 days.

2.8. Bioinformatics analysis of oral mucosal defects after treatment

To further explore the intrinsic molecular mechanisms of wound repair by DCS-RuB$_2$A$_2$-BMSCs, oral wound tissue samples were collected on day 4 for RNA sequencing (RNAseq). The heatmap of differentially expressed genes is shown in Fig. 9A. After administration of the hydrogel, 241 significantly differentially expressed genes (DEGs) were

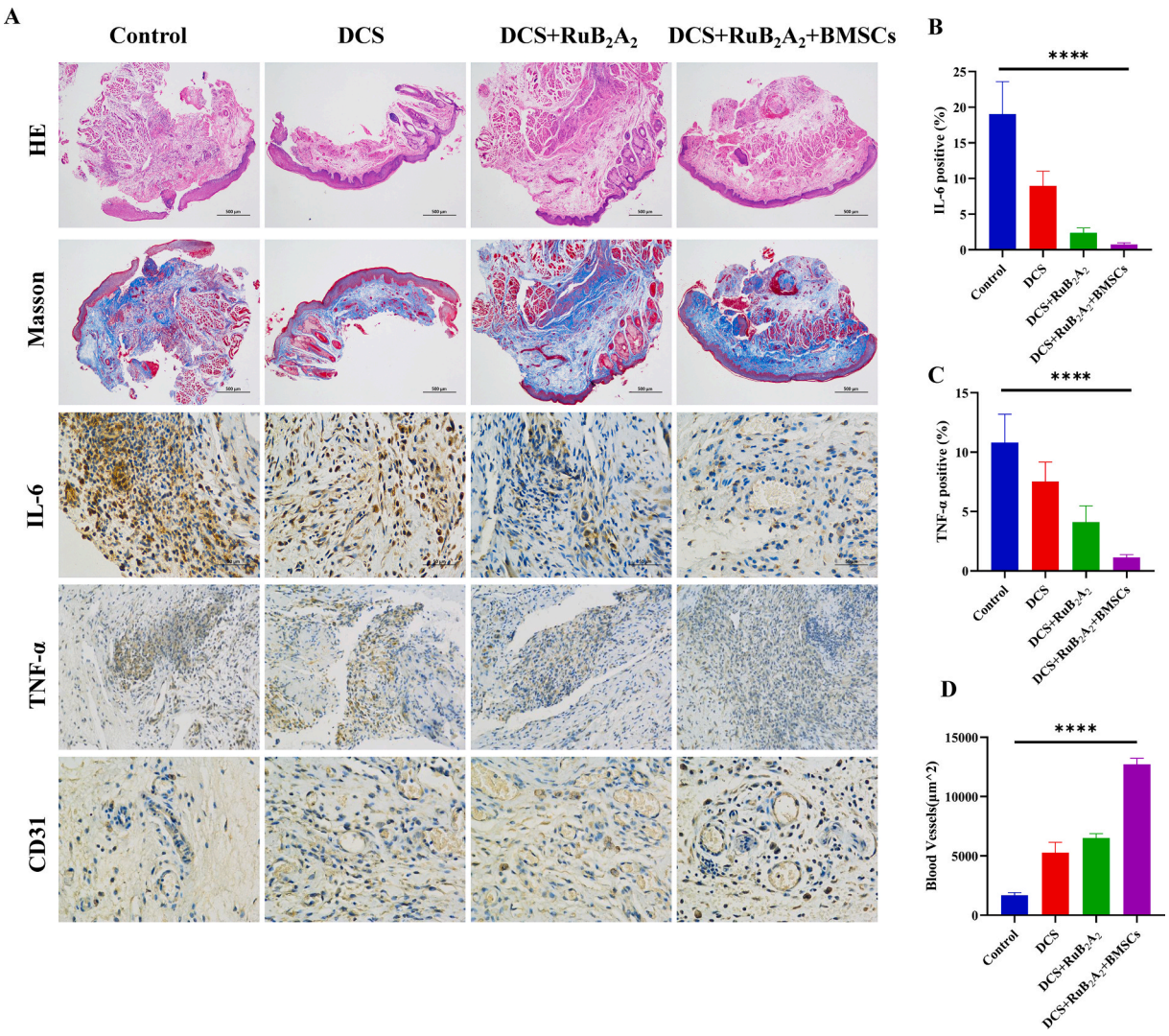

Fig. 8. Histological evaluation of the oral mucosal trauma healing process. (A) Images of H&E and Masson's trichrome staining, in addition to immunochemical staining of the inflammatory factors IL-6 and TNF-α and angiogenesis factors at the wound site in rats treated with different materials for 4 days. (B–D) Quantitation of IL-6, TNF-α, and angiogenesis factor levels in (A) (n ≥ 3, *$p < 0.05$, **$p < 0.01$, ***$p < 0.001$, ****$p < 0.0001$).

identified, 147 of which were upregulated and 94 were downregulated, according to the empirical bayes method (fold change ≥2; p value < 0.05). These include genes closely related to inflammation, such as IL-17b, IL-Z11. A significant difference was found between the transcriptomics profiles of the control and hydrogel-treated groups, and enrichment analysis was conducted based on the DEGs. Hierarchical cluster analysis separated and screened the DEGs between wound tissues from the control and hydrogel-treated rats. Reactome enrichment analysis and reactome annotations analysis demonstrates that the DEGs are mainly involved in the immune system, neutrophil degranulation, hemostasis and extracellular matrix organization (Fig. 9B, Supplementary Figs. 3A and B). These results suggest that wound healing is closely related to these processes, DCS-RuB_2A_2-BMSCs also promoted wound healing by improving these effects. Gene ontology (GO) enrichment analysis and GO annotations analysis revealed a focus on response to biotic stimulus, response to cytokine, cellular response to cytokine stimulus, response to bacterium and virus (Fig. 9C, Supplementary Fig. 3C). This indicated that the rapid wound healing in the DCS-RuB_2A_2-BMSCs group was attributed to the paracrine effect of BMSCs, which greatly promoted the release of growth factors and the killing effect on bacteria and viruses. Kyoto Encyclopedia of Genes and Genomes (KEGG) enrichment analysis and KEGG annotations analysis of DEGs found enrichments in regulation of actin cytoskeleton, bacterial invasion of epithelial cells, viral myocarditis, neutrophil extracellular trap formation and inflammatory mediator regulation of TRP channels (Fig. 9D, Supplementary Fig. 3D. These results suggest that the key enriched items of DEGs are the bacterial invasion of epithelial cells, immune system, metabolism, inflammation improvement concentrated in the extracellular matrix, neutrophil action, cellular action on growth factors, and downstream signaling pathway regulation. This indicates that DCS-RuB_2A_2-BMSCs ameliorates bacterial-induced infections, reduces inflammation due to the paracrine effects of BMSCs, improves the wound microenvironment by regulating cytokines, and promotes wound repair.

3. Conclusions

We designed and constructed a light-responsive antimicrobial hydrogel that can present BMSCs for the topical treatment of oral mucosal wounds. The developed hydrogel is based on dodecyl chitosan, which is loose and porous and possesses good hemostatic and coagulation effects, in addition to being capable of activating platelets to promote wound healing. A light-responsive antibacterial system was constructed using ruthenium bipyridine-crosslinked DCS, which has a larger storage modulus and porosity under dark conditions, and is suitable for the presentation and release of BMSCs. This moist, soft, 3D

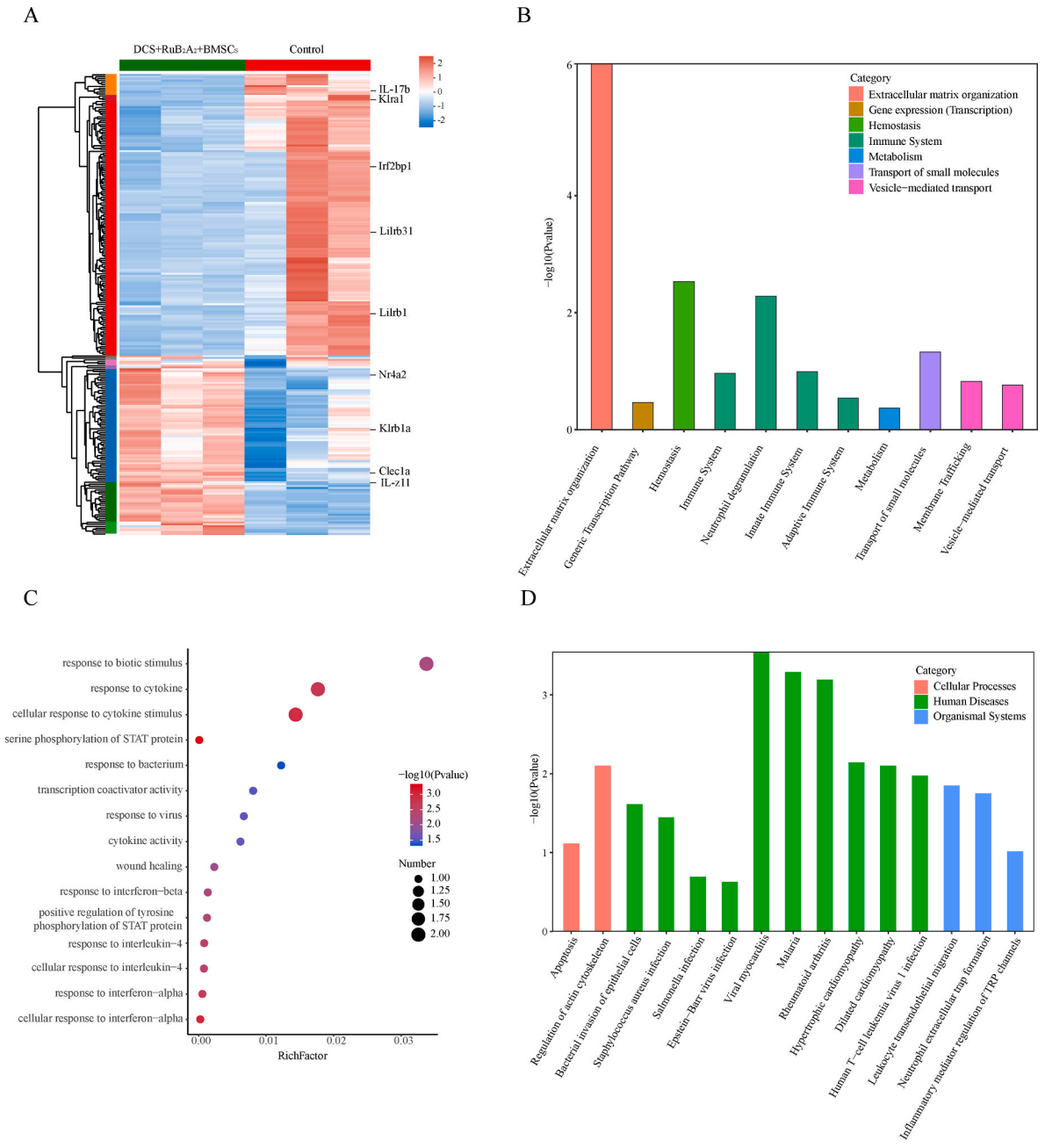

Fig. 9. Global assessment of the wound microenvironment using RNA-seq after treatment with the photoresponse material. (A) Heat map of the upregulated and downregulated genes in the wound microenvironment after treatment with the photoresponse material (fold change $\geq$2 and $p < 0.05$). (B) Reactome enrichment analysis of the DEGs. (C)Gene ontology (GO) enrichment analysis of the DEGs. (D) Kyoto Encyclopedia of Genes and Genomes (KEGG) enrichment analysis of the DEGs.

culture system is conducive to the release of growth factors and cytokines at the wound site. Following exposure to light for a period of time, the pyridine carboxaldehyde in DCS-RuB_2A_2 becomes detached, and RuB_2/RuB_2A is removed from the gel network and anchors to the bacterial membrane with help from the long dodecyl chain of DCS, which plays a local sterilization effect. The system has good biocompatibility and broad-spectrum antibacterial properties. In addition, when combined with the anti-inflammatory and repair-promoting effects of BMSCs, the material can repair oral mucosal wounds in a short period of time. Our study shows that this multifunctional light-responsive hydrogel has commercialization potential and further supports the development of innovative treatments for oral mucosal diseases.

Aging causes skin to become more vulnerable to mechanical damage, in addition to causing changes in skin microbiome, increases in fragmented elastin and collagen, and loss of water, leading to dry skin and increased wrinkles [68]. Accumulation of senescent cells in the elderly leads to increased inflammation, decreased skin immune function, and higher susceptibility to bacterial infections [69,70]. Wound healing is also affected by age, leading to chronic wounds. Clinical data demonstrate that oral mucosal wounds in the elderly recover more slowly than those in younger individuals [71]. Oral infection leads to inflammation, which reduces the capacity of oral mucosal wounds to recover and may even increase the risk of systemic diseases, such as atherosclerosis, coronary heart disease, stroke, chronic obstructive pulmonary disease, diabetes, cancer, and rheumatoid arthritis. Therefore, it is meaningful to research and develop materials to promote oral mucosal healing in aged subjects. Current bioactive materials are used to promote wound contracture and significantly increase collagen

deposition at the injured site, thus accelerating the repair of skin wounds [72,73]. As an effective bactericidal and early anti-inflammatory material, DCS-RuB_2A_2-BMSCs should be further explored to evaluate whether it exerts a significant reparation effect in aged subjects and other severe wound models that are difficult to repair.

4. Experimental section

4.1. Materials

$Ru(bpy)_2Cl_2$ and 3-pyridinecarboxaldehyde were purchased from Beijing Huawei Ruike Chemical Co., Ltd. Paraformaldehyde-glutaraldehyde in PBS was bought from ShanghaiMacklin Biochemical Co., Ltd. Chitosan was obtained from Sigma-Aldrich Co., Ltd. Chloral hydrate was procured from Sangon Biotech (Shanghai) Co., Ltd. Deionized AMTA, N, N-dimethylformamide (DMF), and sodium cyanoborohydride were purchased from Shanghai Aladdin Biochemical Technology Co., Ltd. Anhydrous ethanol (C_2H_5OH) was bought from China Medicine (Group) Shanghai Chemical Reagent Corp.I. All chemical reagents were used as received without further purification. Water (18.2 MΩ cm) obtained from a Milli-Q system (Millipore, Bedford, MA) was used for all experiments.

4.2. Preparation of RuB_2A_2

A mass of 200 mg (0.412 mmol) $Ru(bpy)_2Cl_2$ was dissolved in 10 mL water under argon protection and refluxed for 5 h at 80 °C. A solution of 264 mg (2.472 mmol) 3-pyridinecarbaldehyde in 10 mL ethanol was added dropwise to the above reaction, which was subsequently refluxed overnight. After the reaction, ethanol was removed and the solid was cooled to room temperature. 1 M NH_4PF_6 was added and the solution was extracted with dichloromethane (DCM). The lower organic phase was taken, dried over magnesium sulfate, and filtered, and the solvent was evaporated to dryness to obtain a brown-red solid. A DCM to methanol ratio of 6:1 was used as the eluent for silica gel chromatography column separation to remove excess 3-pyridinecarboxaldehyde, and the pure orange-red solution was collected. The solvent was evaporated to dryness, and methanol was subsequently used as the solvent to pass through a chloride ion-exchange column. Methanol was evaporated to dryness to yield the final product as a brown-red solid.

4.3. Synthesis of dodecyl-modified chitosan (DCS)

The synthesis of DCS was performed based on previous work with some modifications. Specifically, 1 g chitosan (CS) was added to 50 mL 2% acetic acid aqueous solution at room temperature with stirring to dissolve. To make the reaction more homogeneous, different amounts of dodecanal (molar ratio of dodecanal to chitosan: 0.1:1, 0.2:1, 0.3:1, 0.4:1, 0.6:1, 0.8:1) was dissolved in 40 mL ethanol, and this solution was then added to the chitosan solution under constant stirring until it had dissolved. Subsequently, excessive sodium borohydride ($NaBH_4$:CS = 3:1) was added to this mixture in small amounts and stirred at room temperature until it dissolved. An appropriate amount of sodium hydroxide (NaOH) solution was added to adjust the pH of the mixed solution to 7.0, which was then stirred at room temperature overnight. The following day, the precipitated DCS was washed at least three times with 70–100% ethanol until the pH value was neutral. Finally, the precipitates were dried to obtain DCS powder.

4.4. In vitro antibacterial assay of DCS-RuB_2A_2

Taking *Escherichia coli and Staphylococcus aureus* (*E. coli* and *S. aureus*) as model bacteria, the antibacterial ability of RuB_2A_2 at different concentrations was assessed using the spread plate count method. After mixing 5 mL bacterial suspension (10^4 CFU/mL) with different concentrations of RuB_2A_2, the mixture was spread evenly on nutrient agar plates. After culture at 37 °C for 18 h, the plate was photographed and the number of colonies were recorded. The effect of light on the bacteriostatic properties of the hydrogel and RuB_2A_2 was evaluated using the zone of inhibition (ZOI) method. A 100-μL aliquot of bacterial suspension (10^4 CFU/mL) was spread evenly on each nutrient agar plate, after which the hydrogel and its components were placed on top. After culture at 37 °C for 18 h, the RuB_2A_2 and 0.4 DCS + RuB_2A_2 groups were treated with light at the same time, and the size of the ZOI was observed.

4.5. Animals

C57BL/6 mice and SD rats (6–8 weeks old) were purchased from Vital River Laboratory Animal Technology (Shanghai, China). All animals were bred and maintained under specific pathogen-free conditions. Animal use and experimental procedures were approved by the Animal Care and Use Committee of Shanghai University. The HEK 293T cell line was obtained from the Cell Culture Center of the Chinese Academy of Medical Sciences.

4.6. Isolation and culture of cells

Isolation and culture of BMSCs was performed as previously reported [74,75]. The isolated cells and HEK 293T cells were cultured in complete DM/F12 (Thermo Scientific, Gibco) and DMEM (Biological Industries) supplemented with 10% FBS (Thermo Scientific, Gibco).

4.7. Mouse tail hemostasis test

A similar hemostatic procedure was performed in a mouse tail amputation model. Approximately 50% was cut off the length of the tail, and the blood was allowed to drip onto a pre-weighed filter paper. Subsequently, the mouse tails were inserted into tubes containing hydrogels with differing degrees of substitution, and the tail blood was gently absorbed. The tails were removed every 30 s to absorb the blood with filter paper, and images were taken. A group treated with gauze served as a control. Blood loss and time to hemostasis were monitored.

4.8. Blood clotting time (BCT)

An equal amount of CS or DCS was placed in a glass vial, preheated with the extracted blood at 37 °C for 5 min, and then 200 μL blood was added to the surface of the material. $CaCl_2$ (25 mM) was pipetted into the tube and incubated at 37 °C. Timing from this point, the tube was tilted every 30 s until the blood had completely coagulated; this is the BCT. Each group was measured at least three times.

4.9. Cytotoxicity assessment of the hydrogel and its components

HEK 293T cells were seeded at 4×10^3 cells per well (in 100 μL) on a 96-well plate and allowed to attach for 24 h. Different materials were then added to the wells and incubated for a further 24 h. The CCK-8 test was used to determine the cell viability in the experimental group and expressed as a percentage of viable cells relative to the control.

Hoechst 33342/propidium iodide (PI) double staining assay: For live and dead cell visualization, HEK 293T (1×10^5) cells were seeded on a cover slip in a 24-well plate with different gel treatments under 5% CO_2 at 37 °C. After 24 h of incubation, the supernatant was removed, and cells were washed with cold PBS. HEK 293T cells were labeled with Hoechst 33342 and PI at 37 °C for 20 min, after which the cells were washed three times with PBS and visualized using a Leica fluorescence microscope (Germany).

4.10. Oral mucosal trauma model construction

Male SD rats (average weight 200 g) were anesthetized by

intraperitoneal injection of 7% chloral hydrate (0.1 mL/10 g). Trauma was established on the oral mucosa of rats using a dental drill (round, approximately 5 mm in diameter), and the wound was then infected with 20 μL 10^8 CFU/mL *E. coli* and *S. aureus*. After 1 h, the experimental group was treated with hydrogel samples, while the control group was treated with saline. On days 0, 1, 2, and 4 after induction of the wound, photographs of the different groups were taken using a camera at a fixed height to record the size and appearance of the wounds. The wound closure rate was calculated using the following formula: Wound closure rate (%) = $(A_0 - A_T)/A_0 \times 100\%$

4.11. Immunohistochemistry

To evaluate epidermal regeneration and inflammation at the wound site, skin tissue from the wound was obtained after the mice were sacrificed. The wound tissues were fixed in 4% neutral formaldehyde solution at room temperature for 24 h, embedded in paraffin, and cut into 4-μm sections. The sections were soaked in xylene for 15 min to remove the paraffin, and then rehydrated through a graded alcohol series. After antigen retrieval in 10 mM citrate buffer (pH 6) for 10–15 min at 100 °C, endogenous peroxidase activity was blocked with 3% hydrogen peroxide for 10 min. The sections were soaked in blocking solution for a further 60–90 min. Subsequently, the tissue sections were stained with hematoxylin and eosin (H&E) solution and incubated overnight at 4 °C in a humidified box with specific primary antibodies against IL-6, TNF-α, and CD31. The following day, the sections were incubated with a secondary antibody for 1 h, developed with DAB chromogenic substrate for 10 min, and counterstained with hematoxylin for 1 min. All sections were evaluated under a light microscope.

4.12. Statistical analysis

Data are expressed as the mean ± SD. Comparisons between groups were assessed using a Student's *t*-test, one-way ANOVA, and Tukey's multiple comparisons test. Statistical data were analyzed using the Graphpad Prism 8 software. Differences were considered statistically significant at $^*p < 0.05$, $^{**}p < 0.01$, $^{***}p < 0.001$, $^{****}p < 0.0001$.

Declaration of competing interest

The authors declare no competing interests.

CRediT authorship contribution statement

Wenxin Qi: Conceptualization, Experimental operation, Investigation, Formal analysis, Data curation, Writing – original draft, Writing – review & editing. **Naijun Dong:** Image creation, Methodology, Experimental operation, Review. **Lingling Wu:** Experimental operation, Formal analysis, Investigation, Writing. **Xueqi Zhang:** Methodology, Writing, Formal analysis. **He Li:** Methodology, Writing, Formal analysis. **Hao Wu:** Methodology, Writing, Formal analysis. **Natalie Ward:** Writing – review & editing. **Jian Yu:** Writing, Formal analysis. **He Liu:** Writing, Formal analysis. **Jiao Wang:** Project administration, Project design, Funding acquisition, Writing – review & editing, Supervision, Project administration. **Xiaoyong Deng:** Project administration, Project design, Funding acquisition, Writing – review & editing, Supervision, Project administration. **Robert Chunhua Zhao:** Project administration, Project design, Funding acquisition, Writing – review & editing, Supervision, Project administration.

Acknowledgments

This work was sponsored by The CAMS Innovation Fund for Medical Sciences (2022-I2M-1-012), National Key Research and Development Program of China (2020YFA0113000, 2018YFA0109800), Basic Research Program of Shanghai (20JC1412200), National Natural Science Foundation of China (81971324).

Appendix A. Supplementary data

Supplementary data to this article can be found online at https://doi.org/10.1016/j.bioactmat.2022.10.027.

References

[1] M.A. Peres, B. Daly, C.C. Guarnizo-Herreno, H. Benzian, R.G. Watt, Oral diseases: a global public health challenge - authors' reply, Lancet 395 (10219) (2020) 186–187, https://doi.org/10.1016/S0140-6736(19)32997-6.
[2] H. An, Z. Gu, L. Zhou, S. Liu, C. Li, M. Zhang, Y. Xu, P. Zhang, Y. Wen, Janus mucosal dressing with a tough and adhesive hydrogel based on synergistic effects of gelatin, polydopamine, and nano-clay, Acta Biomater. 149 (2022) 126–138, https://doi.org/10.1016/j.actbio.2022.07.016.
[3] D.J. Lin, L.S. Yang, L.L. Wen, H.Z. Lu, Q.M. Chen, Z. Wang, Crosstalk between the oral microbiota, mucosal immunity, and the epithelial barrier regulates oral mucosal disease pathogenesis, Mucosal Immunol. 14 (6) (2021) 1247–1258, https://doi.org/10.1038/s41385-021-00413-7.
[4] F. D'Aiuto, D. Gable, Z. Syed, Y. Allen, K.L. Wanyonyi, S. White, J.E. Gallagher, Evidence summary: the relationship between oral diseases and diabetes, Br. Dent. J. 222 (12) (2017) 944–948, https://doi.org/10.1038/sj.bdj.2017.544.
[5] X. Qi, W. Lin, Y. Wu, Q. Li, X. Zhou, H. Li, Q. Xiao, Y. Wang, B. Shao, Q. Yuan, Cbd promotes oral ulcer healing via inhibiting cmpk2-mediated inflammasome, J. Dent. Res. 101 (2) (2022) 206–215, https://doi.org/10.1177/00220345211024528.
[6] J.R. Naglik, A. Konig, B. Hube, S.L. Gaffen, Candida albicans-epithelial interactions and induction of mucosal innate immunity, Curr. Opin. Microbiol. 40 (2017) 104–112, https://doi.org/10.1016/j.mib.2017.10.030.
[7] Y. Li, K. Wang, B. Zhang, Q. Tu, Y. Yao, B. Cui, B. Ren, J. He, X. Shen, J.D. Van Nostrand, J. Zhou, W. Shi, L. Xiao, C. Lu, X. Zhou, Salivary mycobiome dysbiosis and its potential impact on bacteriome shifts and host immunity in oral lichen planus, Int. J. Oral Sci. 11 (2) (2019) 13, https://doi.org/10.1038/s41368-019-0045-2.
[8] K. Wang, W.X. Lu, Q.C. Tu, Y.C. Ge, J.Z. He, Y. Zhou, Y.P. Gou, J.D. Van Nostrand, Y.J. Qin, J.Y. Li, J.Z. Zhou, Y. Li, L.Y. Xiao, X.D. Zhou, Preliminary analysis of salivary microbiome and their potential roles in oral lichen planus, Sci Rep-Uk 6 (2016), https://doi.org/10.1038/srep22943.
[9] Z. Yang, Q. Cui, R. An, J. Wang, X. Song, Y. Shen, M. Wang, H. Xu, Comparison of microbiomes in ulcerative and normal mucosa of recurrent aphthous stomatitis (ras)-affected patients, BMC Oral Health 20 (1) (2020) 128, https://doi.org/10.1186/s12903-020-01115-5.
[10] S. ElAoud, A. Kamoun, N. Mahfoudh, A. Charfi, M. Snoussi, H. Hachicha, A. Jerbi, C. Dammak, F. Frikha, F. Hakim, L. Gaddour, Z. Bahloul, H. Makni, Beyond human leukocyte antigen class i antigens: hereditary hemochromatosis gene mutations in recurrent aphthous oral ulcers and behcet disease in the south of Tunisia, Med. Princ. Pract. 26 (5) (2017) 427–432, https://doi.org/10.1159/000481782.
[11] E. Marlina, B. Hirani, V. Mercadante, M. Shephard, A. Smith, P028 the anti-inflammatory effects of a poly-probiotic on the oral mucosa, Journal of Crohn s and Colitis 14 (Supplement_1) (2020) S145–S146, https://doi.org/10.1093/ecco-jcc/jjz203.157.
[12] C.C. Villar, A. Dongari-Bagtzoglou, Fungal diseases: oral dysbiosis in susceptible hosts, Periodontology 87 (1) (2000) 166–180, https://doi.org/10.1111/prd.12378, 2021.
[13] J.G. Barin, M.V. Talor, J.A. Schaub, N.L. Diny, X. Hou, M. Hoyer, N.K. Archer, E. S. Gebremariam, M.F. Davis, L.S. Miller, N.R. Rose, D. Cihakova, Collaborative interferon-gamma and interleukin-17 signaling protects the oral mucosa from staphylococcus aureus, Am. J. Pathol. 186 (9) (2016) 2337–2352, https://doi.org/10.1016/j.ajpath.2016.07.001.
[14] Y.H. Li, C.H. Wang, S.S. Jean, F.L. Chen, W.S. Lee, J.H. Chang, Lemierre syndrome complicating deep neck infection and descending necrotizing mediastinits caused by odontogenic infections, J. Microbiol. Immunol. Infect. 53 (2) (2020) 357–359, https://doi.org/10.1016/j.jmii.2019.10.002.
[15] C. Pagano, S. Giovagnoli, L. Perioli, M.C. Tiralti, M. Ricci, Development and characterization of mucoadhesive-thermoresponsive gels for the treatment of oral mucosa diseases, Eur. J. Pharmaceut. Sci. 142 (2020), https://doi.org/10.1016/j.ejps.2019.105125.
[16] M. Duran-Lobato, Z. Niu, M.J. Alonso, Oral delivery of biologics for precision medicine, Adv. Mater. 32 (13) (2020), e1901935, https://doi.org/10.1002/adma.201901935.
[17] Y. Han, S. Xu, J. Jin, X. Wang, X. Liu, H. Hua, X. Wang, H. Liu, Primary Clinical Evaluation of Photodynamic Therapy with Oral Leukoplakia in Chinese Patients, vol. 9, 2019, https://doi.org/10.3389/fphys.2018.01911.
[18] A. Andisheh-Tadbir, A. Yaghoubi, N. Tanideh, M. Mardani, The effect of indocyanine green-mediated photodynamic therapy in healing of experimentally induced oral mucosal traumatic ulcer in rat, Laser Med. Sci. 36 (3) (2021) 611–618, https://doi.org/10.1007/s10103-020-03096-x.
[19] W. Liang, Q. Lu, F. Yu, J. Zhang, C. Xiao, X. Dou, Y. Zhou, X. Mo, J. Li, M. Lang, A multifunctional green antibacterial rapid hemostasis composite wound dressing for wound healing, Biomater. Sci. 9 (21) (2021) 7124–7133, https://doi.org/10.1039/d1bm01185e.

[20] Y. Bu, L. Zhang, G. Sun, F. Sun, J. Liu, F. Yang, P. Tang, D. Wu, Tetra-peg based hydrogel sealants for in vivo visceral hemostasis, Adv. Mater. 31 (28) (2019), e1901580, https://doi.org/10.1002/adma.201901580.
[21] J. Liu, J. Li, F. Yu, Y.X. Zhao, X.M. Mo, J.F. Pan, In situ forming hydrogel of natural polysaccharides through schiff base reaction for soft tissue adhesive and hemostasis, Int. J. Biol. Macromol. 147 (2020) 653–666, https://doi.org/10.1016/j.ijbiomac.2020.01.005.
[22] H. Geng, Q. Dai, H. Sun, L. Zhuang, A. Song, F. Caruso, J. Hao, J. Cui, Injectable and sprayable polyphenol-based hydrogels for controlling hemostasis, ACS Appl. Bio Mater. 3 (2) (2020) 1258–1266, https://doi.org/10.1021/acsabm.9b01138.
[23] M. Long, Y. Zhang, P. Huang, S. Chang, Y.H. Hu, Q. Yang, L.F. Mao, H.M. Yang, Emerging nanoclay composite for effective hemostasis, Adv. Funct. Mater. 28 (10) (2018), https://doi.org/10.1002/adfm.201704452.
[24] Y.F. Ma, J.X. Yao, Q. Liu, T. Han, J.P. Zhao, X.H. Ma, Y.M. Tong, G.R. Jin, K. Qu, B. Q. Li, F. Xu, Liquid bandage harvests robust adhesive, hemostatic, and antibacterial performances as a first-aid tissue adhesive, Adv. Funct. Mater. 30 (39) (2020), https://doi.org/10.1002/adfm.202001820.
[25] Z.J. Xu, B. Liang, J.Z. Tian, J. Wu, Anti-inflammation biomaterial platforms for chronic wound healing, Biomater Sci-Uk 9 (12) (2021) 4388–4409, https://doi.org/10.1039/d1bm00637a.
[26] W.J. Huang, Y.X. Wang, Y. Chen, Y.T. Zhao, Q. Zhang, X. Zheng, L.Y. Chen, L. N. Zhang, Strong and rapidly self-healing hydrogels: potential hemostatic materials, Adv Healthc Mater 5 (21) (2016) 2813–2822, https://doi.org/10.1002/adhm.201600720.
[27] B. Liu, R.Z. Fu, Z.G. Duan, C.H. Zhu, J.J. Deng, D.D. Fan, Ionic liquid-based non-releasing antibacterial, anti-inflammatory, high-transparency hydrogel coupled with electrical stimulation for infected diabetic wound healing, Compos. B Eng. 236 (2022), https://doi.org/10.1016/j.compositesb.2022.109804.
[28] J.A. del Olmo, L.P. Alvarez, V. Saez-Martinez, S. Benito-Cid, L. Ruiz-Rubio, R. Perez-Gonzalez, J.L. Vilas-Vilela, J.M. Alonso, Wound healing and antibacterial chitosan-genipin hydrogels with controlled drug delivery for synergistic anti-inflammatory activity, Int. J. Biol. Macromol. 203 (2022) 679–694, https://doi.org/10.1016/j.ijbiomac.2022.01.193.
[29] H. Hu, F.J. Xu, Rational design and latest advances of polysaccharide-based hydrogels for wound healing, Biomater Sci-Uk 8 (8) (2020) 2084–2101, https://doi.org/10.1039/d0bm00055h.
[30] A. Cerqueira, F. Romero-Gavilán, I. García-Arnáez, C. Martinez-Ramos, S. Ozturan, R. Izquierdo, M. Azkargorta, F. Elortza, M. Gurruchaga, J. Suay, I. Goñi, Characterization of magnesium doped sol-gel biomaterial for bone tissue regeneration: the effect of mg ion in protein adsorption, Mater Sci Eng C Mater Biol Appl 125 (2021), 112114, https://doi.org/10.1016/j.msec.2021.112114.
[31] L. Wang, D. Zhang, Y. Ren, S. Guo, J. Li, S. Ma, M. Yao, F. Guan, Injectable hyaluronic acid hydrogel loaded with bmsc and ngf for traumatic brain injury treatment, Mater Today Bio 13 (2022), 100201, https://doi.org/10.1016/j.mtbio.2021.100201.
[32] R. Zhu, T. Yan, Y. Feng, Y. Liu, H. Cao, G. Peng, Y. Yang, Z. Xu, J. Liu, W. Hou, X. Wang, Z. Li, L. Deng, S. Wang, J. Li, Q. Han, H. Li, G. Shan, Y. Cao, X. An, J. Yan, Z. Zhang, H. Li, X. Qu, J. Zhu, S. Zhou, J. Wang, F. Zhang, J. Gao, R. Jin, D. Xu, Y. Q. Ma, T. Huang, S. Peng, Z. Zheng, I. Stambler, E. Gilson, L.W. Lim, A. Moskalev, A. Cano, S. Chakrabarti, B. Ulfhake, H. Su, H. Xu, S. Xu, F. Wei, H.M. Brown-Borg, K.J. Min, G. Ellison-Hughes, C. Caruso, K. Jin, R.C. Zhao, Mesenchymal stem cell treatment improves outcome of covid-19 patients via multiple immunomodulatory mechanisms, Cell Res. 31 (12) (2021) 1244–1262, https://doi.org/10.1038/s41422-021-00573-y.
[33] X. Xiao, M. Xu, H. Yu, L. Wang, X. Li, J. Rak, S. Wang, R.C. Zhao, Mesenchymal stem cell-derived small extracellular vesicles mitigate oxidative stress-induced senescence in endothelial cells via regulation of mir-146a/src, Signal Transduct. Targeted Ther. 6 (1) (2021) 354, https://doi.org/10.1038/s41392-021-00765-3.
[34] G. Ren, L. Zhang, X. Zhao, G. Xu, Y. Zhang, A.I. Roberts, R.C. Zhao, Y. Shi, Mesenchymal stem cell-mediated immunosuppression occurs via concerted action of chemokines and nitric oxide, Cell Stem Cell 2 (2) (2008) 141–150, https://doi.org/10.1016/j.stem.2007.11.014.
[35] J. Huo, S. Sun, Z. Geng, W. Sheng, R. Chen, K. Ma, X. Sun, X. Fu, Bone marrow-derived mesenchymal stem cells promoted cutaneous wound healing by regulating keratinocyte migration via β2-adrenergic receptor signaling, Mol. Pharm. 15 (7) (2018) 2513–2527, https://doi.org/10.1021/acs.molpharmaceut.7b01138.
[36] Z.F. Han, J.H. Cao, Z.Y. Liu, Z. Yang, R.X. Qi, H.L. Xu, Exosomal lncrna klf3-as1 derived from bone marrow mesenchymal stem cells stimulates angiogenesis to promote diabetic cutaneous wound healing, Diabetes Res. Clin. Pract. 183 (2022), 109126, https://doi.org/10.1016/j.diabres.2021.109126.
[37] L. Guo, J. Du, D.F. Yuan, Y. Zhang, S. Zhang, H.C. Zhang, J.W. Mi, Y.L. Ning, M. J. Chen, D.L. Wen, J.H. Sun, D. Liu, L. Zeng, A. Zhang, J. Jiang, H. Huang, Optimal h2o2 preconditioning to improve bone marrow mesenchymal stem cells' engraftment in wound healing, Stem Cell Res. Ther. 11 (1) (2020) 434, https://doi.org/10.1186/s13287-020-01910-5.
[38] R. Tutuianu, A.M. Rosca, D.M. Iacomi, M. Simionescu, I. Titorencu, Human mesenchymal stromal cell-derived exosomes promote in vitro wound healing by modulating the biological properties of skin keratinocytes and fibroblasts and stimulating angiogenesis, Int. J. Mol. Sci. 22 (12) (2021), https://doi.org/10.3390/ijms22126239.
[39] R.C. Cheung, T.B. Ng, J.H. Wong, W.Y. Chan, Chitosan: an update on potential biomedical and pharmaceutical applications, Mar. Drugs 13 (8) (2015) 5156–5186, https://doi.org/10.3390/md13085156.
[40] X. Zhao, B. Guo, H. Wu, Y. Liang, P.X. Ma, Injectable antibacterial conductive nanocomposite cryogels with rapid shape recovery for noncompressible hemorrhage and wound healing, Nat. Commun. 9 (1) (2018) 2784, https://doi.org/10.1038/s41467-018-04998-9.
[41] V. Patrulea, V. Ostafe, G. Borchard, O. Jordan, Chitosan as a starting material for wound healing applications, Eur. J. Pharm. Biopharm. 97 (2015) 417–426, https://doi.org/10.1016/j.ejpb.2015.08.004.
[42] T. Phuangkaew, N. Booranabunyat, S. Kiatkamjornwong, P. Thanyasrisung, V. P. Hoven, Amphiphilic quaternized chitosan: synthesis, characterization, and anti-cariogenic biofilm property, Carbohydr. Polym. 277 (2022), 118882, https://doi.org/10.1016/j.carbpol.2021.118882.
[43] Y. Zhang, J. Guan, J.M. Wu, S. Ding, J. Yang, J.H. Zhang, A.J. Dong, L.D. Deng, N-alkylated chitosan/graphene oxide porous sponge for rapid and effective hemostasis in emergency situations, Carbohydr. Polym. 219 (2019) 405–413, https://doi.org/10.1016/j.carbpol.2019.05.028.
[44] M.A. Khan, M. Mujahid, A review on recent advances in chitosan based composite for hemostatic dressings, Int. J. Biol. Macromol. 124 (2019) 138–147, https://doi.org/10.1016/j.ijbiomac.2018.11.045.
[45] L. Yu, X. Shang, H. Chen, L. Xiao, Y. Zhu, J. Fan, A tightly-bonded and flexible mesoporous zeolite-cotton hybrid hemostat, Nat. Commun. 10 (1) (2019) 1932, https://doi.org/10.1038/s41467-019-09849-9.
[46] L.J. Pei, Z.S. Cai, S.B. Shang, Z.Q. Song, Synthesis and antibacterial activity of alkylated chitosan under basic ionic liquid conditions, J. Appl. Polym. Sci. 131 (7) (2014), https://doi.org/10.1002/app.40052.
[47] P. Deng, W. Jin, Z. Liu, M. Gao, J. Zhou, Novel multifunctional adenine-modified chitosan dressings for promoting wound healing, Carbohydr. Polym. 260 (2021), 117767, https://doi.org/10.1016/j.carbpol.2021.117767.
[48] Y. Zheng, N. Pan, Y. Liu, X. Ren, Novel porous chitosan/n-halamine structure with efficient antibacterial and hemostatic properties, Carbohydr. Polym. 253 (2021), 117205, https://doi.org/10.1016/j.carbpol.2020.117205.
[49] Z. Chen, X. Yao, L. Liu, J. Guan, M. Liu, Z. Li, J. Yang, S. Huang, J. Wu, F. Tian, M. Jing, Blood coagulation evaluation of n-alkylated chitosan, Carbohydr. Polym. 173 (2017) 259–268, https://doi.org/10.1016/j.carbpol.2017.05.085.
[50] Y. Huang, Y. Zhang, L. Feng, L. He, R. Guo, W. Xue, Synthesis of n-alkylated chitosan and its interactions with blood, Artif. Cell Nanomed. Biotechnol. 46 (3) (2018) 544–550, https://doi.org/10.1080/21691401.2017.1328687.
[51] B. Shagdarova, A. Lunkov, A. Il'ina, V. Varlamov, Investigation of the properties of n-[(2-hydroxy-3-trimethylammonium) propyl] chloride chitosan derivatives, Int. J. Biol. Macromol. 124 (2019) 994–1001, https://doi.org/10.1016/j.ijbiomac.2018.11.209.
[52] D.T. Vo, C.K. Lee, Antimicrobial sponge prepared by hydrophobically modified chitosan for bacteria removal, Carbohydr. Polym. 187 (2018) 1–7, https://doi.org/10.1016/j.carbpol.2018.01.082.
[53] X. Wang, J. Guan, X. Zhuang, Z. Li, S. Huang, J. Yang, C. Liu, F. Li, F. Tian, J. Wu, Z. Shu, Exploration of blood coagulation of n-alkyl chitosan nanofiber membrane in vitro, Biomacromolecules 19 (3) (2018) 731–739, https://doi.org/10.1021/acs.biomac.7b01492.
[54] X.X. Zhang, G.P. Chen, L.J. Cai, Y.T. Wang, L.Y. Sun, Y.J. Zhao, Bioinspired pagoda-like microneedle patches with strong fixation and hemostasis capabilities, Chem. Eng. J. 414 (2021), https://doi.org/10.1016/j.cej.2021.128905.
[55] Y. Liang, Z. Li, Y. Huang, R. Yu, B. Guo, Dual-dynamic-bond cross-linked antibacterial adhesive hydrogel sealants with on-demand removability for post-wound-closure and infected wound healing, ACS Nano 15 (4) (2021) 7078–7093, https://doi.org/10.1021/acsnano.1c00204.
[56] J. Wu, H. Yuk, T.L. Sarrafian, C.F. Guo, L.G. Griffiths, C.S. Nabzdyk, X. Zhao, An off-the-shelf bioadhesive patch for sutureless repair of gastrointestinal defects, Sci. Transl. Med. 14 (630) (2022), eabh2857, https://doi.org/10.1126/scitranslmed.abh2857.
[57] T.L. Rapp, C.B. Highley, B.C. Manor, J.A. Burdick, I.J. Dmochowski, Ruthenium-crosslinked hydrogels with rapid, visible-light degradation, Chemistry 24 (10) (2018) 2328–2333, https://doi.org/10.1002/chem.201704580.
[58] S. Theis, A. Iturmendi, C. Gorsche, M. Orthofer, M. Lunzer, S. Baudis, A. Ovsianikov, R. Liska, U. Monkowius, I. Teasdale, Metallo-supramolecular gels that are photocleavable with visible and near-infrared irradiation, Angew. Chem., Int. Ed. 56 (50) (2017) 15857–15860, https://doi.org/10.1002/anie.201707321.
[59] M. Sitohy, A.R. Al-Mohammadi, A. Osman, S. Abdel-Shafi, N. El-Gazzar, S. Hamdi, S.H. Ismail, G. Enan, Silver-protein nanocomposites as antimicrobial agents, Nanomaterials 11 (11) (2021), https://doi.org/10.3390/nano11113006.
[60] B.A. Edhari, M. Mashreghi, A. Makhdoumi, M. Darroudi, Antibacterial and antibiofilm efficacy of ag nps, ni nps and al(2)o(3) nps singly and in combination against multidrug-resistant klebsiella pneumoniae isolates, J. Trace Elem. Med. Biol. 68 (2021), 126840, https://doi.org/10.1016/j.jtemb.2021.126840.
[61] S. Cao, Q. Li, S. Zhang, Z. Liu, X. Lv, J. Chen, Preparation of biodegradable carboxymethyl cellulose/dopamine/ag nps cryogel for rapid hemostasis and bacteria-infected wound repair, Int. J. Biol. Macromol. 222 (Pt A) (2022) 272–284, https://doi.org/10.1016/j.ijbiomac.2022.09.172.
[62] C. Mari, V. Pierroz, R. Rubbiani, M. Patra, J. Hess, B. Spingler, L. Oehninger, J. Schur, I. Ott, L. Salassa, S. Ferrari, G. Gasser, DNA intercalating ruii polypyridyl complexes as effective photosensitizers in photodynamic therapy, Chem. Eur J. 20 (44) (2014) 14421–14436, https://doi.org/10.1002/chem.201402796.
[63] Y. Wang, Q. Zhou, Y. Wang, J. Ren, H. Zhao, S. Wu, J. Yang, J. Zhen, Y. Luo, X. Wang, Y. Gu, In vitro photodynamic inactivation effects of ru(ii) complexes on clinical methicillin-resistant staphylococcus aureus planktonic and biofilm cultures, Photochem. Photobiol. 91 (1) (2015) 124–133, https://doi.org/10.1111/php.12378.
[64] Y. Zhang, Q. Zhou, N. Tian, C. Li, X. Wang, Ru(ii)-complex-based DNA photocleaver having intense absorption in the phototherapeutic window, Inorg.

Chem. 56 (4) (2017) 1865–1873, https://doi.org/10.1021/acs.inorgchem.6b02459.
[65] J. Shen, A.A. Nada, N.Y. Abou-Zeid, S.M. Hudson, Synthesis of chitosan iodoacetamides via carbodiimide coupling reaction: effect of degree of substitution on the hemostatic properties, Carbohydr. Polym. 229 (2020), 115522, https://doi.org/10.1016/j.carbpol.2019.115522.
[66] G.M. DiSalvo, A.R. Robinson, M.S. Aly, E.R. Hoglund, S.M. O'Malley, J. C. Griepenburg, Polymersome poration and rupture mediated by plasmonic nanoparticles in response to single-pulse irradiation, Polymers 12 (10) (2020), https://doi.org/10.3390/polym12102381.
[67] W. Peng, D. Li, K. Dai, Y. Wang, P. Song, H. Li, P. Tang, Z. Zhang, Z. Li, Y. Zhou, C. Zhou, Recent progress of collagen, chitosan, alginate and other hydrogels in skin repair and wound dressing applications, Int. J. Biol. Macromol. 208 (2022) 400–408, https://doi.org/10.1016/j.ijbiomac.2022.03.002.
[68] E.S. Chambers, M. Vukmanovic-Stejic, Skin barrier immunity and ageing, Immunology 160 (2) (2020) 116–125, https://doi.org/10.1111/imm.13152.
[69] B.M. Hall, V. Balan, A.S. Gleiberman, E. Strom, P. Krasnov, L.P. Virtuoso, E. Rydkina, S. Vujcic, K. Balan, I. Gitlin, K. Leonova, A. Polinsky, O.B. Chernova, A. V. Gudkov, Aging of mice is associated with p16(ink4a)- and β-galactosidase-positive macrophage accumulation that can be induced in young mice by senescent cells, Aging (Albany NY) 8 (7) (2016) 1294–1315, https://doi.org/10.18632/aging.100991.
[70] M.C.R.d. Castro, M. Ramos-e-Silva, Cutaneous infections in the mature patient, Clin. Dermatol. 36 (2) (2018) 188–196, https://doi.org/10.1016/j.clindermatol.2017.10.010.
[71] C.G. Engeland, J.A. Bosch, J.T. Cacioppo, P.T. Marucha, Mucosal wound healing: the roles of age and sex, Arch. Surg. 141 (12) (2006) 1193–1197, https://doi.org/10.1001/archsurg.141.12.1193. ; discussion 1198.
[72] A. Hernández-Rangel, E.S. Martin-Martinez, Collagen based electrospun materials for skin wounds treatment, J. Biomed. Mater. Res. 109 (9) (2021) 1751–1764, https://doi.org/10.1002/jbm.a.37154.
[73] M.C. Catoira, L. Fusaro, D. Di Francesco, M. Ramella, F. Boccafoschi, Overview of natural hydrogels for regenerative medicine applications, J. Mater. Sci. Mater. Med. 30 (10) (2019) 115, https://doi.org/10.1007/s10856-019-6318-7.
[74] D.D. Houlihan, Y. Mabuchi, S. Morikawa, K. Niibe, D. Araki, S. Suzuki, H. Okano, Y. Matsuzaki, Isolation of mouse mesenchymal stem cells on the basis of expression of sca-1 and pdgfr-alpha, Nat. Protoc. 7 (12) (2012) 2103–2111, https://doi.org/10.1038/nprot.2012.125.
[75] X. Liu, X. Qu, Y. Chen, L. Liao, K. Cheng, C. Shao, M. Zenke, A. Keating, R.C. Zhao, Mesenchymal stem/stromal cells induce the generation of novel il-10-dependent regulatory dendritic cells by socs3 activation, J. Immunol. 189 (3) (2012) 1182–1192, https://doi.org/10.4049/jimmunol.1102996.